Long-Range Electron Transfer in Zinc-Phthalocyanine-Oligo(Phenylene-ethynylene)-Based Donor-Bridge-Acceptor Dyads

ARTICLE *in* INORGANIC CHEMISTRY · OCTOBER 2012

Impact Factor: 4.76 · DOI: 10.1021/ic3013552 · Source: PubMed

Inorganic Chemistry

Article

pubs.acs.org/IC

Long-Range Electron Transfer in Zinc-Phthalocyanine-Oligo(Phenylene-ethynylene)-Based Donor-Bridge-Acceptor Dyads

Erik Göransson,[†] Julien Boixel,[‡] Jérôme Fortage,[‡] Denis Jacquemin,*[,‡,§] Hans-Christian Becker,[†] Errol Blart,[‡] Leif Hammarström,*[,†] and Fabrice Odobel*[,‡]

[†]Physical Chemistry, Department of Chemistry - Ångström, Uppsala University, Box 523, 751 20 Uppsala, Sweden

[‡]LUNAM Université, Université de Nantes, CNRS, Chimie et Interdisciplinarité: Synthèse, Analyse, Modélisation (CEISAM), UMR 6230; 2, rue de la Houssinière − BP 92208 − 44322 Nantes Cedex 3, France

[§]Institut Universitaire de France, 103 blvd St Michel, 75005 Paris Cedex 5, France

Supporting Information

ABSTRACT: In the context of long-range electron transfer for solar energy conversion, we present the synthesis, photophysical, and computational characterization of two new zinc(II) phthalocyanine oligophenylene-ethynylene based donor-bride-acceptor dyads: **ZnPc-OPE-AuP$^+$** and **ZnPc-OPE-C$_{60}$**. A gold(III) porphyrin and a fullerene has been used as electron accepting moieties, and the results have been compared to a previously reported dyad with a tin(IV) dichloride porphyrin as the electron acceptor (Fortage et al. *Chem. Commun.* **2007**, 4629). The results for **ZnPc-OPE-AuP$^+$** indicate a remarkably strong electronic coupling over a distance of more than 3 nm. The electronic coupling is manifested in both the absorption spectrum and an ultrafast rate for photoinduced electron transfer ($k_{PET} = 1.0 \times 10^{12}$ s^{-1}). The charge-shifted state in **ZnPc-OPE-AuP$^+$** recombines with a relatively low rate ($k_{BET} = 1.0 \times 10^9$ s^{-1}). In contrast, the rate for charge transfer in the other dyad, **ZnPc-OPE-C$_{60}$**, is relatively slow ($k_{PET} = 1.1 \times 10^9$ s^{-1}), while the recombination is very fast ($k_{BET} \approx 5 \times 10^{10}$ s^{-1}). TD-DFT calculations support the hypothesis that the long-lived charge-shifted state of **ZnPc-OPE-AuP$^+$** is due to relaxation of the reduced gold porphyrin from a porphyrin ring based reduction to a gold centered reduction. This is in contrast to the faster recombination in the tin(IV) porphyrin based system ($k_{BET} = 1.2 \times 10^{10}$ s^{-1}), where the excess electron is instead delocalized over the porphyrin ring.

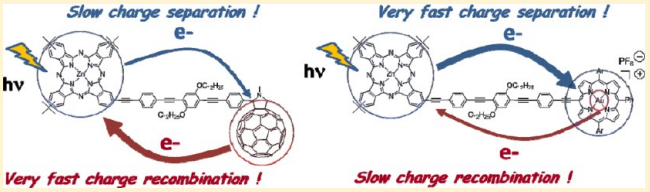

INTRODUCTION

Electron transfer is a central reaction in many biological systems[1] as well as in many molecular devices for solar energy conversion.[2] In biological systems, electron transfer occurs in the initial steps of both Photosystem I and Photosystem II,[3] in the electron transport between iron−sulfur clusters in hydrogenases[4] and along amino acid side chains in proteins.[1a,5] In artificial systems photoinduced electron transfer is a fundamental step to convert solar energy into electricity or into fuels. For example, organic bulk heterojunction solar cells,[6] dye sensitized solar cells,[7] and artificial photosynthetic systems for solar fuels production,[8] all rely on light driven charge-separation. Furthermore, in the emerging field of molecular electronics the electron transfer is the key step that propagates the electronic signal between the different components. There are hopes that molecular systems can be designed to function not only as electronic[9] or photonic wires[10] but also as components such as diodes and switches[11] for more advanced electronic devices.

Investigations of photoinduced charge separation in model systems is particularly valuable to better understand electron transfer in biological and artificial systems and to assist the design of new artificial systems. Understanding of long-range, photoinduced electron transfer has been greatly advanced in recent years, and bridge structures with very small distance dependencies have been found.[12] However, most of these investigations have been on donor-bridge-acceptor systems with fairly weak electronic coupling between the three components, and thus valuable information could be gained from complementary studies of long-range electron transfer in systems with high intercomponent electronic coupling.[13] Furthermore, while electron transfer has been extensively studied in zinc porphyrin based systems,[2a,14] the use of zinc phthalocyanines (ZnPc) is much less explored.[15] Zinc phthalocyanine is a fairly easily oxidized dye, which makes it a good electron donor, and it displays a strong absorption band in the red domain of the visible spectrum.[15d,16] This feature nicely complements the absorption of common light harvesting dyes, which tend to absorb in the blue or green part of the visible spectrum.[17] Herein we present two new donor-bridge-acceptor dyads, designed to undergo long-range photoinduced electron transfer using zinc phthalocyanine as the chromophore and electron donor. We have linked the zinc phthalocyanine to established electron acceptors: a gold(III) porphyrin (AuP$^+$)[13d,18] or a pyrrolidino functionalized fullerene (C_{60})

Received: June 25, 2012

   dx.doi.org/10.1021/ic3013552 | *Inorg. Chem.* XXXX, XXX, XXX−XXX

Chart 1. Structures of the Donor–Acceptor Dyads Described in This Study

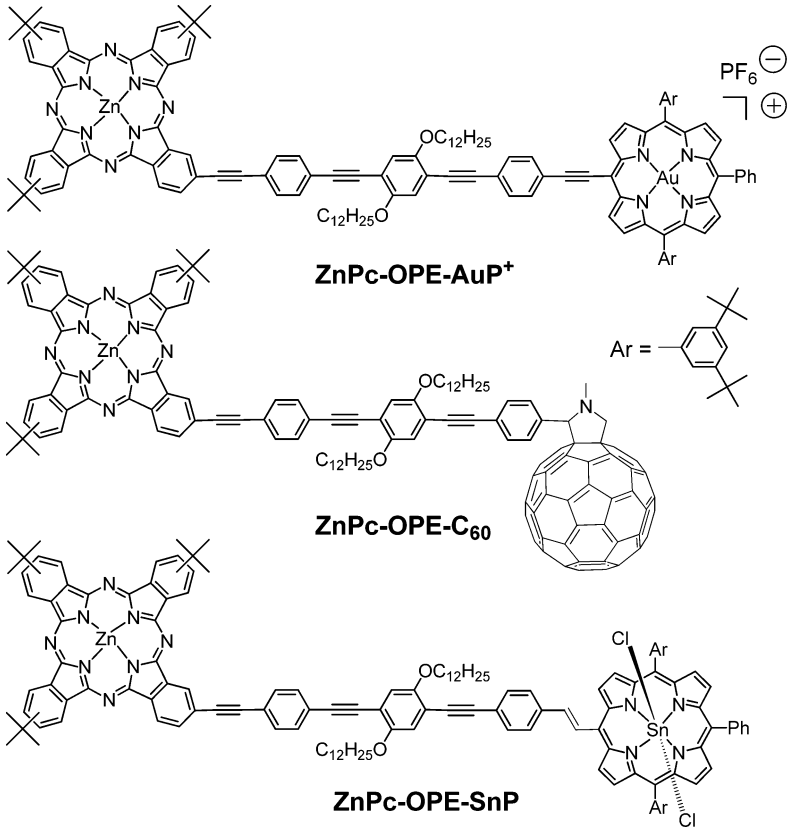

(Chart 1).[14e,g,19] An oligo(phenylene-ethylene) bridge (OPE) was used to link the donor (ZnPc) and acceptor (C_{60} or AuP^+). This type of bridging unit has been shown to mediate electron transfer over long distances[14f–h,20] and when connected through an ethynylene group to the donor and acceptor units this occurs with surprisingly high rates.[13c,d,21] These two new dyads are compared with our earlier investigation, where the acceptor was a tin(IV) dichloride porphyrin (SnP).[13a] Our data strongly suggest that the reduction of a gold porphyrin first occurs on the macrocycle ($Au^{III}P^{\bullet}$) but that the system then relaxes, resulting in a metal based reduction ($Au^{II}P$). This particular feature of gold porphyrin has a profound impact on the forward and backward electron transfer rates compared to the dyads with C_{60} and SnP acceptors and can be used as a tool to engineer rectifying molecular systems in which the kinetics of the charge recombination is much slower than the forward electron transfer.

EXPERIMENTAL SECTION

Synthesis. Compounds **ZnPc-OPE 1**,[13a] halogeno gold porphyrin **3**,[13d] 2,5-didodecyl-1,4-diiodobenzene **5**,[22] 1-ethynyl-4-(trimethylsilylethynyl)benzene **4**,[13d] 4-ethynyl benzaldehyde **6**[23] and iodo-zinc phthalocyanine **9**[24] were prepared according to literature methods. Chemicals were purchased from Aldrich, Acros and used as received. Air sensitive reactions were carried out under argon in dry solvents and glassware.

^{1}H and ^{13}C NMR spectra were recorded on a Bruker ARX 300 MHz or AMX 400 MHz Bruker spectrometer. Chemical shifts for ^{1}H NMR spectra are referenced relative to residual protium in the deuterated solvent ($CDCl_3$ δ = 7.26 ppm for ^{1}H and δ = 77.16 ppm for ^{13}C). EI mass spectra were recorded on an EI-MS HP 5989A spectrometer. MALDI-TOF analyses were performed on a Bruker Ultraflex III, micrOTOF Q spectrometer in positive linear mode at 20 kV acceleration voltage with 2,5-dihydroxybenzoic acid (DHB) or dithranol as matrix. Thin-layer chromatography (TLC) was performed on aluminum sheets precoated with Merck 5735 Kieselgel 60F_{254}. Column chromatography was carried out either with Merck 5735 Kieselgel 60F (0.040–0.063 mm mesh) or with SDS neutral alumina (0.05–0.2 mm mesh).

Compound 2. Compound **1** (**ZnPc-OPE**) (38 mg, 23.9 μmol) was dissolved in THF (2.5 mL) and Bu_4NF (57.3 μL, 1 M in THF) was added. The solution was stirred at room temperature for 2 h. The THF was removed and CH_2Cl_2 was added. The organic phase was washed with water, dried over $MgSO_4$, and concentrated to dryness, affording a green solid (34 mg, 100%). ^{1}H NMR δ (300 MHz, $CDCl_3$, 25 °C): 0.84 (m, 6H, CH_3), 1.24 (m, 36H, CH_2), 1.67 (s, 27H, tBu), 1.78–1.82 (m, 4H, CH_2), 3.12 (s, 1H, H ethynyl), 3.96 (m, 4H, CH_2), 6.90–6.95 (m, 2H, H OPE), 7.40 (m, 4H, H OPE), 7.58 (m, 4H, H OPE), 7.60–7.69 (m, 3H, ZnPc), 7.80–8.10 (m, 9H, ZnPc); MALDI-TOF: *m/z*: calcd for $C_{94}H_{100}N_8O_2Zn$, 1437.733 $[M+H]^+$; found 1437.62 $[M+H]^+$. HR-MS: (ESI): *m/z*: calcd for $C_{94}H_{100}N_8O_2Zn$, 1437.7333 $[M+H]^+$; found 1437.7286 $[M]^+$.

OPE Spacer 7. Compounds **6** (240 mg, 1.86 mmol), **5** (1 g, 1.43 mmol), **4** (368 mg, 1.86 mmol), $PdCl_2$ (50 mg, 0.28 mmol), PPh_3 (112 mg, $4.3.10^{-5}$ mol), $Cu(OAc)_2$ (14 mg, $7.1.10^{-5}$ mol), diisopropylamine (0.5 mL), and triethylamine (13 mL) were dissolved in dry THF (13 mL). The solution was degassed and stirred at 80 °C for 20 h. After cooling down to room temperature, the crude reaction mixture was diluted with CH_2Cl_2. The organic phase was washed with water, dried over $MgSO_4$ and evaporated to dryness. The product was purified by column chromatography over silica (petroleum ether/CH_2Cl_2: 1/1), to afford compound **7** as a yellow solid (342 mg, 31%). ^{1}H NMR δ (300 MHz, $CDCl_3$, 25 °C): 0.22 (s, 9H, TMS), 0.89 (m, 6H, CH_3), 1.27 (m, 32H, CH_2), 1.55 (quint., ^{3}J = 6.3 Hz, 4H, CH_2), 1.83 (quint., ^{3}J = 6.8 Hz, 4H, CH_2), 4.04 (t, ^{3}J = 6.3 Hz, 4H, CH_2), 7.01 (s, 2H, H OPE), 7.45 (m, 4H, H OPE), 7.66 (d, ^{3}J = 7.9 Hz, 2H, H OPE), 7.86 (d, ^{3}J = 7.9 Hz, 2H, H OPE), 10.02 (s, 1H, CHO). HR-

dx.doi.org/10.1021/ic3013552 | Inorg. Chem. XXXX, XXX, XXX–XXX

MS (ESI): m/z: calcd for $C_{52}H_{70}O_3Si$, 770.5099 $[M]^+$; found 770.5170 $[M]^+$.

OPE Spacer 8. The spacer **7** (340 mg, 0.44 mmol) and K_2CO_3 (607 mg, 4.4 mmol) were dissolved in a mixture of CH_2Cl_2 (30 mL) and MeOH (40 mL). The solution was stirred at room temperature for 45 min. CH_2Cl_2 was added, and the organic phase was washed with water, dried over $MgSO_4$, and concentrated to dryness, affording **8** as a yellow solid (262 mg, 85%). ^{1}H NMR δ (300 MHz, $CDCl_3$, 25 °C): 0.85 (m, 6H, CH_3), 1.24 (m, 32H, CH_2), 1.56 (quint., ^3J = 6.1 Hz, 4H, CH_2), 1.87 (quint., ^3J = 6.3 Hz, 4H, CH_2), 3.16 (s, 1H, H ethynyl), 4.05 (m, 4H, CH_2), 7.02 (s, 2H, H OPE), 7.47 (s, 4H, H OPE), 7.66 (d, ^3J = 8.1 Hz, 2H, H OPE), 7.86 (d, ^3J = 8.1 Hz, 2H, H OPE), 10.02 (s, 1H, CHO). HR-MS (ESI): m/z: calcd for $C_{49}H_{62}O_3$, 698.4693 $[M]^+$; found 698.4682 $[M]^+$.

Compound 10. In a Schlenk flask were dissolved zinc tri-*tert*-butyl-iodophthalocyanine **9** (160 mg, 0.18 mmol) and the connector **8** (128 mg, 0.18 mmol) in dry piperidine (10 mL), and the mixture was degassed. Triphenylarsine (110 mg, 0.36 mmol) and $Pd_2(dba)_3.CHCl_3$ (55 mg, 54 μmol) were added, and the solution was degassed again. The reaction mixture was stirred at 40 °C overnight under argon. The solvent was removed and CH_2Cl_2 was added. The organic phase was washed with water (twice), dried over $MgSO_4$, and concentrated to dryness. The product was purified by column chromatography over silica gel (petroleum ether/dioxane: 8/2), to afford a green-blue solid (134 mg, 52%). ^{1}H NMR δ (300 MHz, $CDCl_3$, 25 °C): 0.89 (m, 6H, CH_3), 1.29 (m, 36H, CH_2), 1.62 (s, 27H, tBu), 1.84−1.94 (m, 4H, CH_2), 4.06 (m, 4H, CH_2), 6.98−7.02 (m, 2H, H OPE), 7.47 (m, 4H, H OPE), 7.64 (m, 4H, H OPE), 7.75−8.05 (m, 3H, H ZnPc), 8.10−8.80 (m, 9H, H ZnPc), 10.1 (s, 1H, CHO). HR-MS (ESI): m/z: calcd for $C_{93}H_{100}N_8O_3Zn$ 1440.7210, found 1440.7214 $[M]^+$.

Dyad ZnPc-OPE-C_{60}. Compound **10** (65 mg, 0.045 mmol), fullerene (65 mg, 0.09 mmol), and N-methylglycine (40 mg, 0.44 mmol) were dissolved in dry toluene (65 mL), and the mixture was heated at 140 °C overnight. The solvent was removed and CH_2Cl_2 was added. The organic phase was washed twice with water, dried over $MgSO_4$, and concentrated to dryness. The product was purified by column chromatography over silica gel (toluene/dioxane: 9/1), to afford a green-blue solid (30 mg, 30%). ^{1}H NMR δ (300 MHz, THF-d^8, 25 °C): 0.89 (m, 6H, CH_3), 1.31 (m, 59H, 27H tBu + 32H dodecane), 1.85 (m, 4H, CH_2), 1.95 (m, 4H, CH_2), 2.81 (s, 3H, CH_3 pyrrolidinyl), 4.06 (t, ^3J = 6 Hz, 4H, CH_2), 4.26 (d, ^3J = 9.6 Hz, 1H, H pyrrolidinyl), 5.01 (m, 2H, H pyrrolidinyl), 7.08 (s, 1H, H OPE), 7.11 (s, 1H, H OPE), 7.61 (m, 4H, H OPE), 7.66 (m, 4H, H OPE), 8.30 (m, 4H, H ZnPc), 9.30 (m, 4H, H ZnPc), 9.49 (m, 4H, H ZnPc). MALDI TOF: m/z: calcd. for $C_{155}H_{105}N_9O_2Zn$ 2187.7677, found 2187.7713 $[M]^+$.

Dyad ZnPc-OPE-AuP$^+$. The compound **2** (23 mg, 19.7 μmol), the gold porphyrin **3** (34 mg, 23.7 μmol), $Pd(dppf)Cl_2$ (3 mg, 4 μmol), and CuI (1 mg, 4 μmol) were dissolved in dry Et_3N (1.1 mL) and dry DMF (4.8 mL). The solution was degassed and stirred under argon at 60 °C for 15 h. CH_2Cl_2 was added, and the organic phase was washed with water (3 times), dried over $MgSO_4$, and concentrated. The product was purified by column chromatography over silica (CH_2Cl_2 100% then MeOH/CH_2Cl_2: 2/98), to afford a green solid (22 mg, 44%). ^{1}H NMR δ (300 MHz, $CDCl_3$, 25 °C): 0.84 (m, 6H, CH_3), 1.24 (m, 36H, CH_2), 1.59 (s, 36H, tBu), 1.67 (s, 27H, tBu), 1.78−1.85 (m, 4H, CH_2), 4.00−4.30 (m, 4H, CH_2), 7.00−7.20 (m, 2H, H OPE), 7.40−8.25 (m, 22H, 3H ZnPc + 4H ortho +2H para +5H phenyl +8H OPE), 8.30−8.70 (m, 9H, H ZnPc), 9.00−9.45 (m, 6H, AuP H_β), 10.15−10.17 (m, 2H, AuP H_β). HR-MS (ESI): m/z: calcd for $C_{148}H_{154}N_{12}O_2ZnAu$, 2392.1275 $[M]^+$; found 2392.1278 $[M]^+$.

Electrochemistry. Electrochemical measurements were performed with a potentiostat-galvanostat AutoLab controlled by resident GPES software (General Purpose Electrochemical System 4.9) using a conventional single-compartment three-electrode cell. The working electrode was a Pt electrode, the auxiliary was a Pt wire of 10 mm long, and the reference electrode was the saturated potassium chloride calomel electrode (SCE). The supported electrolyte was 0.1 N Bu_4NPF_6 in dichloromethane, DCM, and the solutions were purged with argon before the measurements. All potentials are quoted relative to SCE. In all the experiments the scan rate was 0.1 V/s.

Spectroscopy. *Absorption and Emission Spectroscopy.* UV−vis absorption spectra were recorded on a Cary 5000 absorption spectrometer, and steady-state emission spectra were measured on a Horiba SPEX Fluorolog 3 fluorimeter. During emission measurements the optical density was kept below 0.1 at the excitation wavelength. The benzonitrile (PhCN) (99%, Fluka) was distilled over phosphorus pentaoxide and filtered through K_2CO_3(s). Using nondistilled benzonitrile resulted in aggregation, which could be observed as a strong perturbation of the ZnPc Q-band.

Absorption spectra of the reduced and oxidized states of the dyads were recorded with a HP diode array spectrometer. Tri-*p*-bromophenyl aminium hexafluorophosphate ($TpBPA^+PF_6^-$, $E^\circ \approx 1.1$ vs SCE)[25] was used as oxidant to form the $ZnPc^{+\bullet}$-OPE-acceptor. The aminium salt was prepared according to the procedure of Rhile et al.[26] As a reductant we used cobaltocene (CoCp2, $E^\circ \approx -1.0$ V vs SCE),[25] allowing for the spectra of the reduced dyads. The cobaltocene was purchased from Sigma-Aldrich (Sweden) as a 10% solution in hexane and used as received. Both the oxidation and the reduction of the dyads were done in a glovebox and deaerated PhCN was used as solvent.

Time-resolved fluorescence was measured with a time-correlated single photon counting setup (TCSPC), using 400 or 405 nm for excitation. The system has previously been described by Habenicht et al.[27] In summary: The 400 nm excitation light was obtained from the frequency doubled output of a Ti-sapphire laser (Coherent RegA 900; 200 kHz repetition rate, λ = 800 nm, fwhm 180 fs) (IRF ~80 ps). For 405 nm excitation a 405 nm diode laser at 5 MHz repetition rate (fwhm 100 ps) was used (IRF ~120 ps). The emission was detected using a Hamamatsu MCP. Magic angle setup was ensured with two polarizers, and scattered excitation light and filter emission was blocked using a combination of a 600 nm cutoff filter and a 751 nm interference filter. The instrument response function (IRF) was measured using a scattering solution of Ludox silica sol in water. That the 400 or 405 nm excitation populates a higher singlet excited state does not affect the observed data since the internal conversion to the lowest ^{1}ZnPc is expected to be much faster than the TCSPC resolution (~40 ps). This is in agreement with the lack of a detectable rise time for the observed ^{1}ZnPc emission at 751 nm.

Femtosecond Transient Absorption (fs-TA). For a detailed description see Petersson et al.[28] Briefly, the output from a Coherent Legend (1 kHz, λ = 800 nm, fwhm 80 fs) was split into a pump and a probe part. Using a TOPAS (Light Conversion) the pump beam was transformed into the desired wavelengths. A 500 Hz chopper was used to block every second pump pulse, and the pump energy was attenuated with neutral density filters so that the pulse energy at the sample was kept between 400 and 600 nJ/pulse (energy variation of the pump energy within a measurement was less than 10%). The timing between the pump and probe pulse was controlled by two different delay lines. For measurements that required subpicosecond time resolution a 30 cm long (~time window ~2 ns) delay line from Physik Intrumente was used, while a 1.5 m (~10 ns) delay line from H2W Technologies was used when a longer time window was necessary. For probing in the UV−visible (350−750 nm), the probe pulse was transformed into a white-light continuum by focusing the 800 nm light into a CaF_2 plate. Residual 800 nm and NIR light was removed by a KG3 filter. For probing in the NIR region (860−1150 nm) a sapphire plate was used to create a broad white light continuum. Visible light was removed using an 800 nm cutoff filter. Detection between 750 and 860 nm is prevented because of excess light from the laser fundamental at 800 nm. The probe light was detected with a silicon photodiode array spectrometer (512 points in a 328 nm wide spectral window). The silicon diodes have a good response at wavelengths below 1000 nm but lose sensitivity at wavelengths longer than 1000 nm, which explains the small signal-to-noise ratio in the NIR measurements. The polarization of the pump was set to ensure magic angle compared to the probe, and the two beams were then focused and overlapped on a ~0.1 mm^2 area inside a 1 mm quartz cuvette.

dx.doi.org/10.1021/ic3013552 | *Inorg. Chem.* XXXX, XXX, XXX−XXX

Scheme 1. Synthesis of the Dyad ZnPc-OPE-AuP^{+}[a]

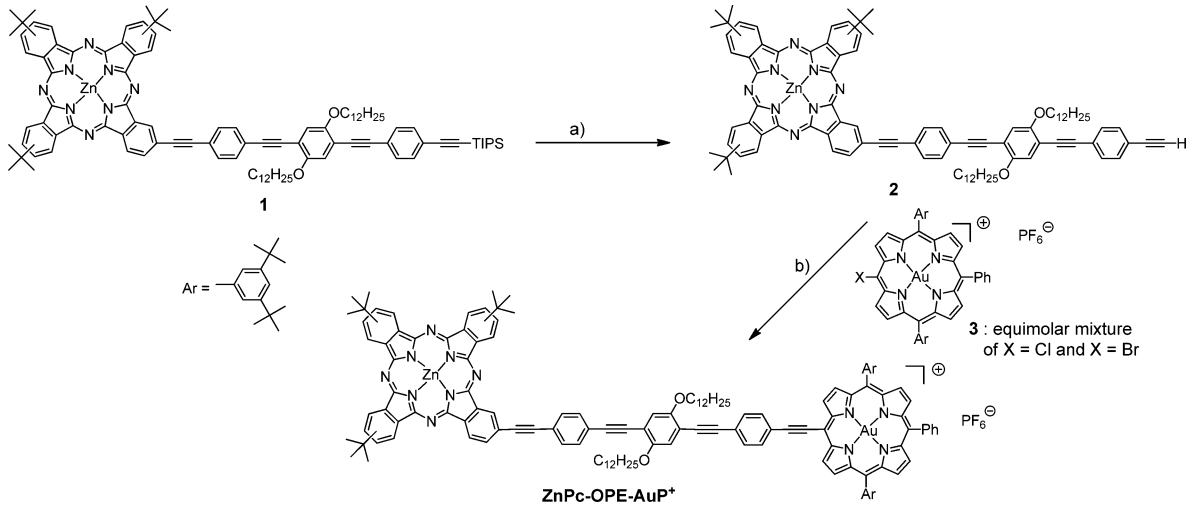

[a]a) Bu_4NF, THF, RT, 100%; b) $Pd(dppf)Cl_2$, CuI, Et_3N, DMF, 60 °C, 43%.

Data analysis of the TCSCP data was done in MATLAB 7, using a model based on a sum of one or two exponential decays, reconvoluted with the experimentally recorded response function. Data from the fs-TA measurements were analyzed with Igor Pro 5.[29] Kinetic data were globally fitted to a sum of exponentials reconvoluted with a Gaussian function to account for the instrument response function. The wavelengths chosen in the global fit were evenly spaced over the observed spectra (every 10th nm for **ZnPc-OPE-AuP^{+}** and every 30th nm for **ZnPc-OPE-C$_{60}$**). The width of the response function and lifetimes were linked between different wavelengths, while time zero and amplitudes of the pre-exponential factors were allowed to vary freely. Each analysis started out from a model of two consecutive reactions (photoinduced electron transfer (PET) followed by back electron transfer (BET)). A third exponential (τ > 100 ns) accounts for the presence of long-lived ^{3}ZnPc, formed in parallel to the ET transition (ISC competing with PET or BET partially resulting in ^{3}ZnPc). However, to achieve a satisfactory global fit a fourth exponential had to be added to the model to account for the presence of unquenched ^{1}ZnPc. The quality of a fit was judged from the residual. Igor Pro reported a standard deviation of the fitted lifetimes to be less than 5%. However by forcibly changing a lifetime, it was noticed that satisfactory fits could be obtained also after changing a lifetime as much as 25% so the overall uncertainty is probably closer to 25%. Examples of fits and residuals can be found in the Supporting Information (SI Figure S4 and SI Figure S5). Following a satisfactory global fit, the obtained response function and lifetimes were used to fit all of the 512 traces, and a decay associated difference spectrum (DADS) was created by plotting the pre-exponential factors against the wavelength for each of the obtained lifetimes. The obtained variation of time zero with wavelength was used to chirp correct the observed difference spectra. To clarify spectral features a smoothing function (second order Savitsky-Golay, 15 points) was applied to difference spectra. Note that no smoothing function was applied on data before kinetic analysis.

DFT Simulations. *Models.* The calculations have been performed on the compounds shown in Chart 1, which have only been slightly simplified by removing the *t*Bu groups of the *Pc* and replacing the $OC_{12}H_{25}$ lateral chains by methoxy groups. As we investigate electronic properties and take into account all π-electrons these simplifications should have only a trifling impact on the computed transition energies. For the AuP^{+} system, the impact of the counterion has been neglected as well. The optimized Cartesian coordinates for the three dyads can be found in the SI. In addition, we have also used specific systems of the acceptor moieties to simulate what follows ET (see discussion around Figure 7). In these acceptor structures, we have simply removed the ZnPc side but conserved the full oligo(phenylene-ethynylene) bridge.

Computational Protocol. To perform DFT and TD-DFT simulations of the structures and properties of the new dyads, the latest commercial version of the Gaussian program has been selected.[30] Default algorithms, parameters, and thresholds have been used, except when otherwise indicated. The computational strategy recently applied to unravel the excited-state properties of inorganic and organic dyes[31] has been adopted. This procedure consists of two sequential steps:

1. The ground-state geometrical parameters have been determined at the PBE0[32]/6-31G(d) level through a force-minimization process. Note that LanL2DZ *pseudo*-potential and basis set have been used for metallic atoms. The bulk solvent (benzonitrile) effects have been included by means of the Polarizable Continuum Model (PCM) in its Integral Equation Formalism (IEF).[33]

2. The first fifteen to twenty lowest-lying excited-states have been determined within the vertical TD-DFT approximation using the CAM-B3LYP[34]/6-31G(d) [LanL2DZ] level of approximation. The choice of CAM-B3LYP, a range-separated hybrid, is dictated by the charge-transfer/long-range nature of the phenomena under investigation. For such states, it is well-recognized that a range-separated hybrid such as CAM-B3LYP offers a physically sound description.[35] As in the first step, the solvent effects have been taken into account at the PCM level of approximation, using a linear-response nonequilibrium model,[36] that is adequate when the reorganization of the solvent is limited to its electronic component (fast processes).

The contour threshold used to represent the molecular orbitals was set to 0.020 au, and a broadening Gaussian presenting a fwhm of 0.35 eV was used to simulate UV/vis spectra from the vertical TD-DFT estimates.

RESULTS AND DISCUSSION

Synthesis of the Dyads. The synthetic route of the dyad **ZnPc-OPE-AuP^{+}** is based on an extension of an earlier procedure previously developed for **ZnPc-OPE-SnP**.[13a] Starting with the known intermediate **ZnPc-OPE-TIPS 1**,[13a] the trisisopropylsilyl group (TIPS) was cleaved with tetrabutylammonium fluoride. The gold porphyrin **3**[13d] was appended to the OPE spacer of the above compound **1** according to a Sonogashira cross-coupling reaction in 43% yield using the catalytic system previously described to prepare bisporphyrin dyads containing a gold porphyrin (Scheme 1).[13a,d] The synthesis of the dyad **ZnPc-OPE-C$_{60}$** required the intermediate spacer **8**, whose synthesis is depicted in Scheme 2. Compound

dx.doi.org/10.1021/ic3013552 | Inorg. Chem. XXXX, XXX, XXX–XXX

Scheme 2. Synthesis of the Dyad ZnPc-OPE-C_{60}[a]

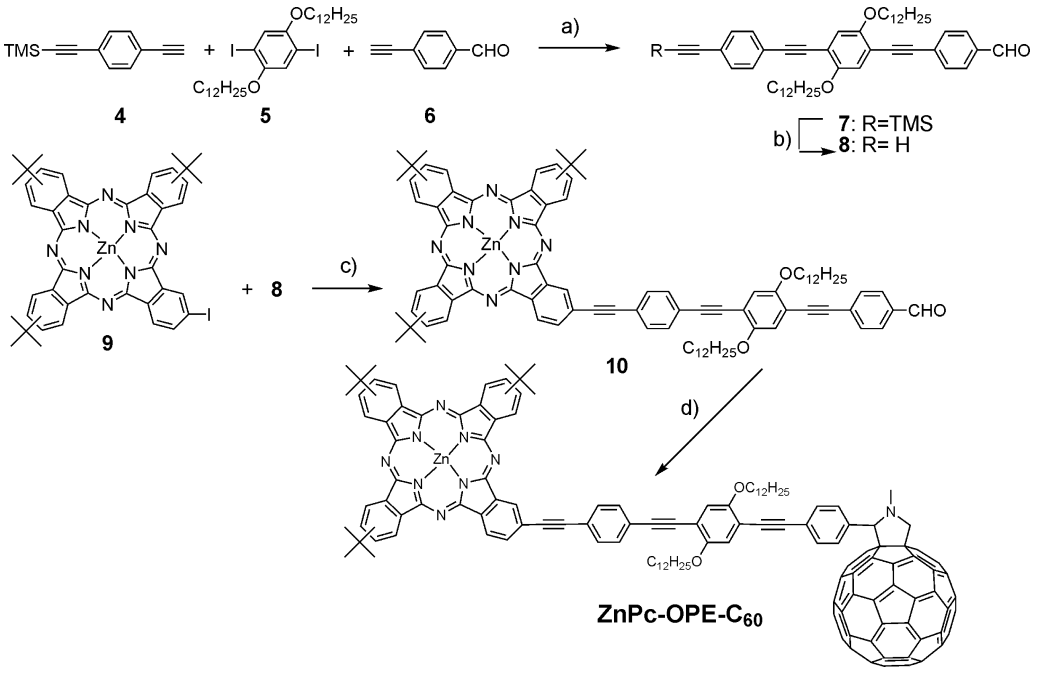

[a]a) $PdCl_2$, PPh_3, $Cu(OAc)_2$, THF, Et_3N, 80°C, 31%; b) K_2CO_3, CH_2Cl_2, MeOH, RT, 85%; c) Pd_2dba_3-$CHCl_3$, $AsPh_3$, piperidine, 40 °C, 52%; d) sarcosine, C_{60}, toluene, reflux, 30%.

Table 1. Electronic Absorption and Emission Properties in Benzonitrile (PhCN) at Room Temperature and Electrochemical Properties in Dichloromethane (DCM) (1 mM $TBAPF_6$)

		emission			$E_{1/2}$ (V vs SCE)		
	absorption λ_{max} (nm)	λ_{max} (nm)[a]	φ_{rel}[b]	τ_{em} (ns)[c]	$ZnPc^{+/0}$	$OPE^{+/0}$	$Acc^{n/n-1}$[d]
ZnPc-OPE[e]	364, 617, 641, 679, 696	705	1.00	1.8[f]	0.46	1.30	
OPE-AuP^{+}[g]	322, 429, 545, 592, 676	[h]	[h]	[h]		1.34	−0.56
ZnPc-OPE-AuP^{+}	388, 549, 597, 681, 698	706	0.22[i]	<0.04[j] *(1.8)*[i]	0.45	1.36	−0.71
ZnPc-OPE-C_{60}	353, 617, 641, 679, 696	705	0.26	0.61 *(1.8)*	0.45	1.28	−0.65
ZnPc-OPE-SnP[e]	355, 438, 579, 618, 642, 679, 696	705	0.05[i]	<0.04[j](1.8)[i]	0.46	1.30	−0.82

[a]Excitation at 680 nm. [b]Relative to ZnPc-OPE emission. [c]Excitation at 400 nm. [d]$Acc^{n/n-1}$ is the first reduction potential of the electron acceptor moiety. [e]Data from Fortage et al.[13a] [f]Corrected from Fortage et al.[13a] [g]From Fortage et al.[13d] [h]Not observed. [i]Most of the observed emission comes from a fraction of [1]ZnPc that is not quenched at all and has the same emission lifetime as the ZnPc-OPE reference, see main text. [j]Lifetime faster than time resolution of TCSPC system.

7 was synthesized in 31% yield by the mixed Sonogashira cross-coupling reaction between the 2,5-didodecyl-1,4-diiodobenzene **5**,[22] the 1-ethynyl-4-(trimethylsilylethynyl)benzene **4**,[13d] and the 4-ethynyl benzaldehyde **6**.[23] The desired compound **7** was easily separated by column chromatography from the symmetrical side-products owing to the large differences of polarity of the three compounds. The TMS group was removed with potassium carbonate, and the spacer **8** was then reacted with iodo-zinc phthalocyanine **9**[24] using classical Sonogashira conditions with this type of reagents (Scheme 2).[13a,d] Finally, the fullerene moiety was grafted on the spacer using Prato reaction following a 1,3-dipolar cyclo-addition between the fullerene and the azomethane ylide formed by the reaction of the aldehyde function of **10** and N-methylglycine.[23,37]

Electrochemistry. The reduction potentials of the dyads were measured with cyclic voltammetry, and the processes were assigned according to the potentials recorded in the reference compounds (Table 1). The first oxidation process occurs on zinc phthalocyanine at around +0.45 V vs SCE, while the oxidation of the OPE spacer is shifted far away into the anodic region at around +1.3 V vs SCE. The three electron acceptors have reduction potentials in a quite narrow potential window, with pyrrolidino-fullerene as the most easily reducible system (−0.65 V vs SCE), followed by the gold porphyrin (−0.71 V vs SCE) and finally by the tin porphyrin (−0.83 V vs SCE). The reduction of the spacer was not accessible in the electroactive window of our experimental conditions (<−1.6 V vs SCE). Note that the $AuP^{+/0}$ potential in **ZnPc-OPE-AuP**$^{+}$ is shifted 0.15 V negative compared to the reference, **OPE-AuP**$^{+}$. This is a sign of strong electronic interaction in the ground state of this dyad (*vide infra*).

Electronic Absorption Spectra. The electronic absorption spectra of the new dyads were recorded in benzonitrile (PhCN), where no aggregation occurs, and are shown together with the relevant reference compounds in Figure 1. The absorption spectrum of **ZnPc-OPE-SnP** can be found in the Supporting Information (SI Figure S1).[13a] The absorption spectrum of **ZnPc-OPE-C_{60}** mainly exhibits features of the ZnPc-moiety (Figure 1a). However, the presence of the C_{60} unit can be seen as an additional feature in the UV region,

dx.doi.org/10.1021/ic3013552 | Inorg. Chem. XXXX, XXX, XXX−XXX

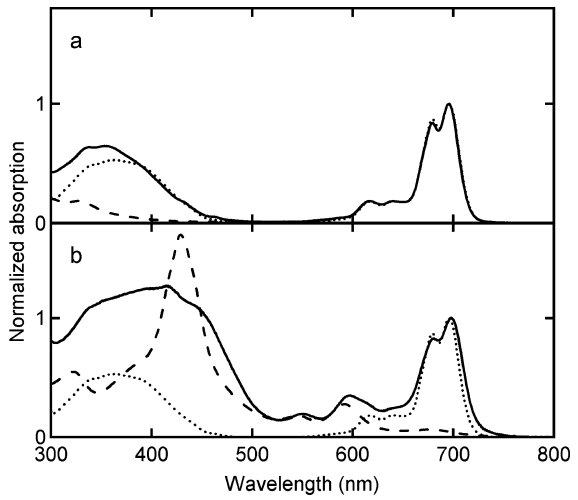

Figure 1. Electronic absorption spectra in benzonitrile at 298 K of a) **ZnPc-OPE-C$_{60}$** (solid line) and its reference compounds **ZnPc-OPE** (dotted line) and **C$_{60}$** (dashed line); b) **ZnPc-OPE-AuP$^+$** (solid line) and its reference compounds **ZnPc-OPE** (dotted line) and **OPE-AuP$^+$** (dashed line). Spectra are normalized to unity intensity of the Q bands.

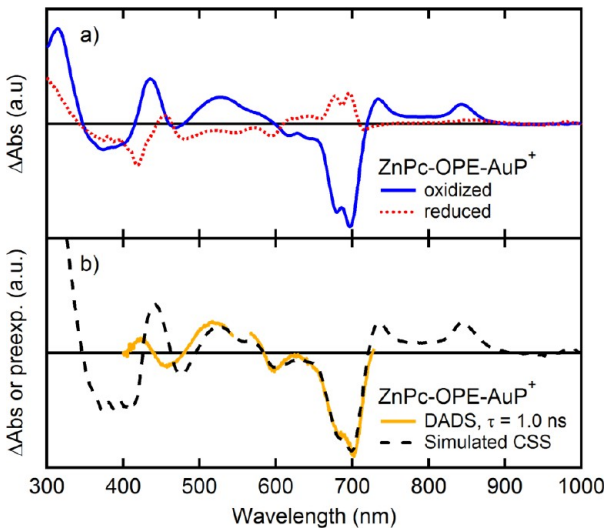

Figure 2. a) Difference spectra of oxidized (blue straight line) and reduced (red dotted line) form of **ZnPc-OPE-AuP$^+$**. b) Simulated difference spectra for the charge shifted state (CSS) of **ZnPc-OPE-AuP$^+$**, created as a sum of the difference spectra of the oxidized and reduced form of **ZnPc-OPE-AuP$^+$**. Overlaid is the decay associated difference spectra (DADS) of the 1.0 ns lifetime observed upon 555 nm excitation of **ZnPc-OPE-AuP$^+$**. The similarity between the two spectra confirms that the 1.0 ns lifetime corresponds to back electron transfer.

causing an apparent blue-shift of the Soret-band compared to that in **ZnPc-OPE**. The splitting of the ZnPc Q-band is most likely caused by the ethynylene linkage, which induces an asymmetry of the otherwise degenerate Q_x- and Q_y-transitions of the ZnPc.[13a,38]

ZnPc-OPE-AuP$^+$ has a more complicated absorption spectrum (Figure 1b). In the Q-band region (500−700 nm) the spectrum of **ZnPc-OPE-AuP$^+$** can be reasonably well described by a sum of the spectra of references **ZnPc-OPE** and **OPE-AuP$^+$**, with only a small red-shift and broadening of the ZnPc Q-band (λ_{max} 698 nm compared to 696 nm in **ZnPc-OPE**). In contrast, the Soret-band region differs significantly from a sum of the reference compounds. Instead of two distinct peaks from the ZnPc and AuP$^+$ Soret-bands there is a strong and very broad peak centered around 400 nm. This shows a strong interaction between the ZnPc and AuP$^+$ moieties, possibly due to excitonic coupling between the Soret-bands or a direct donor−acceptor charge transfer transition (*vide infra*).

Chemical oxidation of **ZnPc-OPE-AuP$^+$**, using tri-*p*-bromophenyl aminium hexafluorophosphate as oxidant, results in the expected disappearance of ground state features and the concomitant growth of ZnPc$^{+\bullet}$ features at 525 nm, 745 nm, and 845 nm around. There is also a sharp absorption peak growing in around 435 nm (Figure 2a), that is not seen in oxidized **ZnPc-OPE**,[13a] but is very similar to the Soret band of **OPE-AuP$^+$**. It thus appears that the perturbation of the gold porphyrin is much weaker when the zinc phthalocyanine is oxidized so that the "normal" AuP$^+$-Soret band is restored. Similarly, one electron reduction of **ZnPc-OPE-AuP$^+$**, using cobaltocene as reductant, results in the appearance of a ground state bleach feature at 420 nm, 550, and 594 nm, and concurrently a new band grows in at 455 nm and the ZnPc Q-bands becomes stronger (Figure 2a). The features at 420 and 455 nm can be explained by a slight red shift of the Soret band, often seen for reduction of Au^{III}P$^+$ to Au^{II}P.[18d,e] The reduction also causes the interaction between gold porphyrin and zinc phthalocyanine to be weaker, explaining the disappearance of the broad Soret band and the slight increase in the ZnPc Q-band.

It is surprising that the interaction between the donor and acceptor is so strong over such a long distance (~23 Å, edge-to-edge). Ethynylene as linking group has indeed been shown to mediate electronic coupling but usually over much shorter distances.[13c,39] Furthermore, in a system with the same bridge and acceptor, but with a zinc porphyrin instead of zinc phthalocyanine as electron donor, we did not observe an interaction of this magnitude.[13d]

Steady-State and Time-Resolved Emission. The emission spectra of **ZnPc-OPE-C$_{60}$** and **ZnPc-OPE-AuP$^+$** (λ_{exc} = 680 nm) are very similar to that of the **ZnPc-OPE** reference, with a $\lambda_{max} \approx$ 705 nm, but with significantly lower quantum yields (SI Figure S2), indicating that electron transfer or some other process is quenching the excited state (*vide infra*). The emission quantum yields relative to **ZnPc-OPE** (φ_{rel}) were determined to 0.26 and 0.22 for **ZnPc-OPE-C$_{60}$** and **ZnPc-OPE-AuP$^+$** respectively (Table 1). **OPE-AuP$^+$** has no detectable emission at room temperature, and there is no indication of C$_{60}$ emission in the **ZnPc-OPE-C$_{60}$** dyad.

The emission lifetime of the lowest singlet excited state (^{1}ZnPc), was determined with time-correlated single photon counting (TCSPC), exciting at 400 nm or at 405 nm. For **ZnPc-OPE-C$_{60}$** two exponential components, τ_1 = 0.61 ns (90%) and τ_2 = 1.8 ns (10%), were necessary to achieve a satisfactory fit of the data. The rate constant for the quenching reaction, k_q, was calculated using eq 1 and the lifetime of the major component, yielding $k_q = 1.1 \times 10^9$ s^{-1} for **ZnPc-OPE-C$_{60}$** in PhCN. The 1.8 ns component is attributed to a fraction of unquenched ^{1}ZnPc-OPE.

$$k_q = \tau_{obs}^{-1} - \tau_0^{1} \quad (1)$$

For **ZnPc-OPE-AuP$^+$** a single 1.8 ns lifetime was observed which is equal to the lifetime of the **^{1}ZnPc-OPE** reference.[13a] However, the much lower emission yield in **ZnPc-OPE-AuP$^+$** indicates that the majority of ZnPc is quenched by a rate faster

dx.doi.org/10.1021/ic3013552 | Inorg. Chem. XXXX, XXX, XXX−XXX

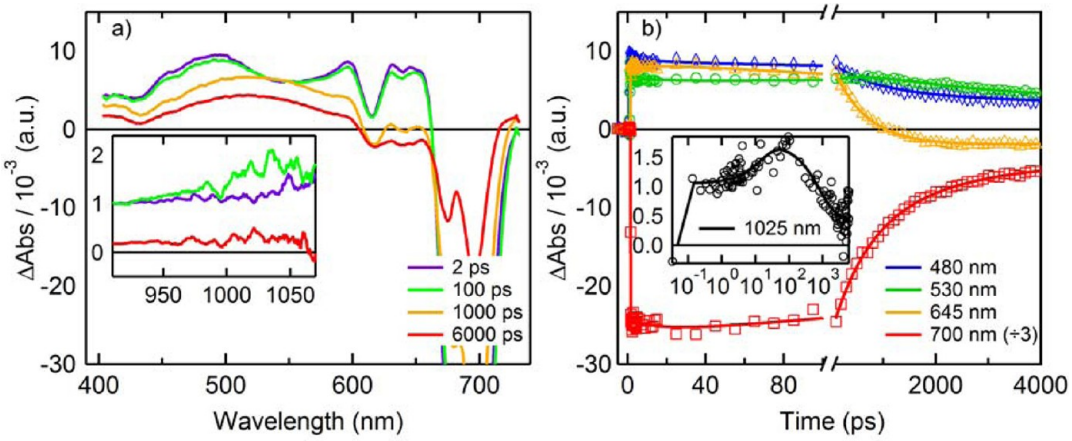

Figure 3. fs-TA measurements on **ZnPc-OPE-C$_{60}$**, excitation at 680 nm. a) Chirp corrected difference spectra at different time points. Inset: Chirp corrected difference spectra in the NIR, showing a band indicative of $C_{60}^{\bullet-}$. The color legend for different time points is valid for both the visible and the NIR spectra. b) Kinetic traces at different wavelengths. Markers are measured data, and solid lines are the results of the global fit to the data (see text).[40] The trace at 700 nm has been scaled down by a factor of 3 to better fit the graph. Inset shows the rise and decay feature of $C_{60}^{\bullet-}$, around 1025 nm (average of 1010−1040 nm) on a logarithmic time scale.

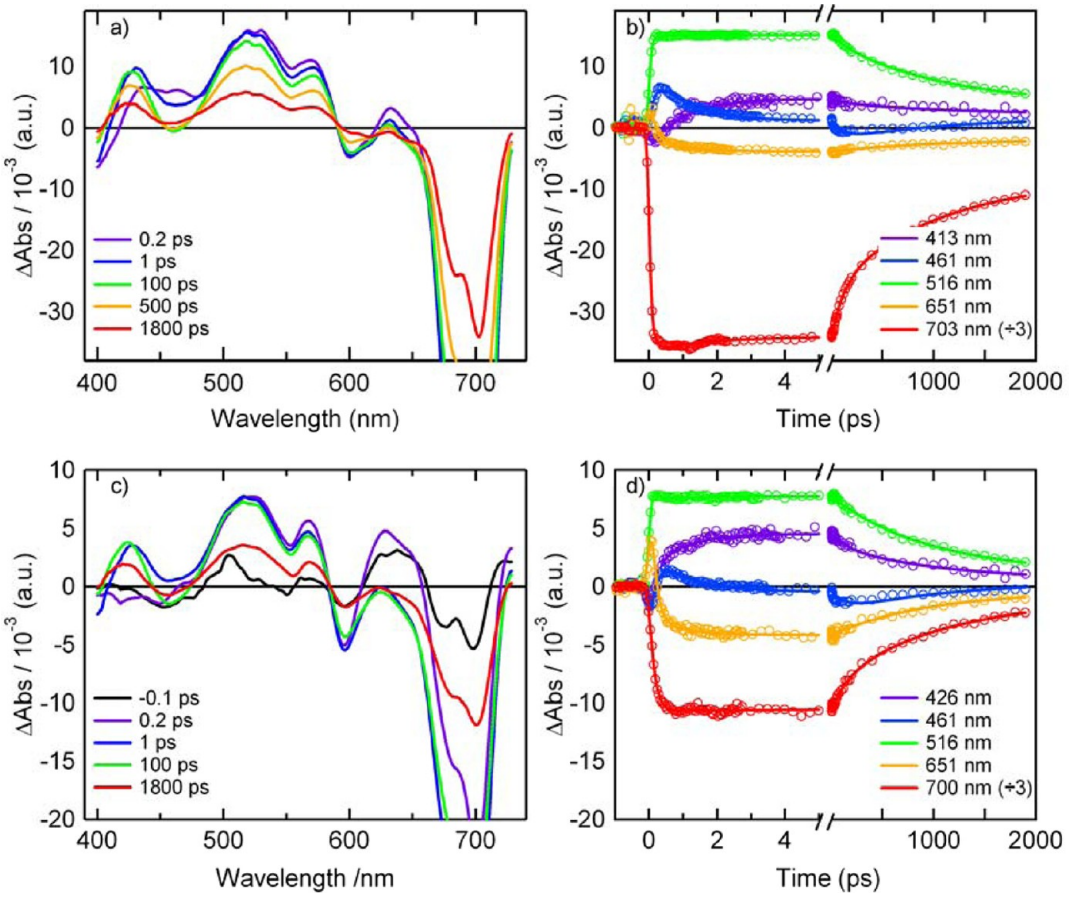

Figure 4. fs-TA measurements on **ZnPc-OPE-AuP$^+$**, excitation at either 680 nm (a and b) or at 555 nm (c and d). Spectra in a and c correspond to transient spectra at a different times after excitation. Kinetic traces at selected wavelengths are shown in b and d. Markers correspond to experimental data, and the solid line is the kinetic fit (see text). The trace at 700 nm has been scaled down by a factor of 3 to better fit the graph.

than the time resolution of the instrument (~40 ps). This means that most of the observed steady-state emission from the **ZnPc-OPE-AuP$^+$** sample comes from a smaller fraction of ^{1}ZnPc (possibly an impurity) which is not quenched at all. This is confirmed by the femtosecond experiments below.

Femtosecond Transient Absorption. Femtosecond pump−probe experiments were performed to follow the photoinduced electron transfer events in **ZnPc-OPE-AuP$^+$** and **ZnPc-OPE-C$_{60}$**.

ZnPc-OPE-C$_{60}$. Figure 3 shows transient absorption data for **ZnPc-OPE-C$_{60}$** at a few time points after a 150 fs excitation pulse at 680 nm (Q-band of ZnPc). The spectrum at early

dx.doi.org/10.1021/ic3013552 | Inorg. Chem. XXXX, XXX, XXX−XXX

times (t < 2 ps) is in very good agreement with that of the lowest singlet exited state (^{1}ZnPc) of **ZnPc-OPE** (SI Figure S3).[13a] ^{1}ZnPc is dominated by a broad absorption band extending over most of the visible region, and superimposed on this band is the ground-state bleach, which creates distinct valleys at 615, 680, and 696 nm. At later delay times (t > 1000 ps) there is a decrease in absorption in the region around 600−670 nm, resulting in a net bleach. This is indicative of ZnPc triplet state (^{3}ZnPc) formation, but the overall rate and yield is not the same as in **ZnPc-OPE**. In a global analysis of ten wavelengths, evenly spaced over the observed spectra ($\Delta\lambda \approx 30$ nm), four lifetimes were needed to fit the observed data; τ = 20 ps, 0.66 ns, 1.8 ns, and ∞ (see SI Figure S4 for example of fits and residuals).[40]

A complementary measurement, probing in the near-infrared (NIR) showed the growth and decay of a broad absorption band between 1000 and 1050 nm.[41] This matches the signature of $C_{60}^{\bullet-}$,[19] which would indicate that the quenching process is photoinduced electron transfer forming the charge-separated state (**ZnPc$^{\bullet+}$-OPE-C$_{60}^{\bullet-}$**). The rise and decay features in the NIR region were globally fitted at 16 wavelengths to lifetimes of ∼15 ps and ∼0.70 ns and ∞, which are similar to the lifetimes observed in the visible region.

The 0.66 ns (UV−vis) and 0.7 ns (NIR) lifetimes matches the fluorescent lifetime (0.61 ns) and is thus assigned to photoinduced charge separation (k_{PET} = 1.1 × 10^9 s^{-1}). Since the shortest lifetime (∼20 ps) also is linked to the $C_{60}^{\bullet-}$ signal, it is reasonable to assign this to the charge recombination reaction ($k_{BET} \approx 5 \times 10^{10}$ s^{-1}). Thus, assuming a reaction scheme with k_{PET} = 1.1 × 10^9 s^{-1} and $k_{BET} \approx 5 \times 10^{10}$ s^{-1} (see Figure 5a), one would expect a maximum concentration of the charge-separated state, **ZnPc$^{\bullet+}$-OPE-C$_{60}^{\bullet-}$**, at ∼80 ps corresponding to only ∼1% of the original excited state population (see SI for details on calculations). The small ratio k_{PET}/k_{BET} explains why the $C_{60}^{\bullet-}$ signal is so low in the NIR region and why there are no clear **ZnPc$^{\bullet+}$** signals in the visible region.[42] The latter causes the 0.66 ns lifetime (charge separation) to appear to mainly result in ground state recovery.

Other quenching mechanisms, such as energy transfer from the ^{1}ZnPc state to the fullerene or enhanced intersystem crossing to the ^{3}ZnPc state, are energetically possible, but based on the absence of transient signals from the long-lived fullerene triplet state[43] and low yield of ^{3}ZnPc these cannot be significant.

ZnPc-OPE-AuP$^+$. Excitation of **ZnPc-OPE-AuP$^+$** at 680 nm results in an initial spectrum (Figure 4a, t = 0.2 ps) which displays a broad transient absorption band, peaking at 520 nm, similar to the band of oxidized **ZnPc-OPE-AuP$^+$**, Figure 2a. Overlaid with this band there are ground state bleach features from the ZnPc Soret band (λ < 450 nm) and the Q-band (650−720 nm). Unexpectedly, there are also additional ground state bleach features from the AuP$^+$ moiety at 400−500 nm, 555 nm, and 620 nm. Combined with the 520 peak, the AuP$^+$ bleach features indicate strong coupling between ZnPc and AuP also in the initial excited state and/or possibly a partial charge transfer absorption.

The initial excited state evolves on a few ps time scale, and a new absorption feature grows in around 420 nm and the bleach at 460 nm becomes more pronounced. Subsequently these new features disappear on the same time scale as the bleach features from the **ZnPc** and **AuP$^+$** Q-bands. A detailed analysis, using a global fit of 30 wavelengths evenly spaced over the observed spectra ($\Delta\lambda \approx 10$ nm), resulted in four lifetimes: 1.2 ps, 0.11 ns, 1.1 ns, and ∞ (held fixed) (see SI Figure S5 for example of fits and residuals). The majority of the ZnPc Q-band bleach recovers with a lifetime of 1.1 ns, but this does not match the emission lifetime (1.8 ns), nor is the magnitude of the ZnPc ground state bleach recovery occurring through the 1.1 ns time component consistent with ^{1}ZnPc decay, because that would have resulted in a larger fluorescence yield than observed. Thus this kinetic process is not the decay of ^{1}ZnPc but rather attributed to back electron transfer from the charge shifted state, **ZnPc$^{\bullet+}$-OPE-Au^{II}P**, to the ground state. This assignment is further supported by the good match between a simulated charge separated state and the decay associated difference spectrum (DADS) of the 1.1 ns component as shown in Figure 2b.[44] From inspection of the decay associated difference spectra of the three remaining time components (SI Figure S7) it was concluded that the 1.2 ps lifetime corresponds to photoinduced electron transfer from ^{1}ZnPc to AuP$^+$. Four lines of evidence support this assignment. 1) The corresponding DADS show changes in the region between 400 and 500 nm, which would be expected from a process that affects AuP$^+$.[43] 2) The 1.2 ps time component barely affects the ground state bleach from the ZnPc Q-band. This is consistent with photoinduced electron transfer since this is a process that does not change the concentration of ground state ZnPc, while it at the same time lowers the concentration of ground state AuP$^+$. 3) Furthermore, the spectral changes in the region between 400 and 500 nm are nicely mirrored in the decay associated difference spectrum of the 1.1 ns component, which makes it very likely that the species created with τ = 1.2 ps (photoinduced electron transfer) disappears with τ = 1.1 ns (back electron transfer), see reaction scheme in Figure 5b. 4) Lastly, observed emission lifetimes and steady-state emission yield suggest that the majority of the ^{1}ZnPc in the **ZnPc-OPE-AuP$^+$** sample reacts with a lifetime that is faster than 40 ps.

For the remaining two time components the 0.11 ps lifetime had too small and unspecific features to be attributed to a specific process, while the "infinite" time component was attributed to a small fraction of unquenched ^{1}ZnPc states evolving into long-lived ^{3}ZnPc states.[45]

Like in our previous study on **ZnPc-OPE-SnP**[13a] we were also interested in the reaction induced by selective excitation of the AuP$^+$ Q(1,0)-band at 555 nm. In the **OPE-AuP$^+$** reference a strong absorption band appears in the region above 600 nm (SI Figure S6). For symmetric gold porphyrins, the lowest singlet excited state (^{1}AuP$^+$) undergoes very rapid intersystem crossing to the lowest triplet state (^{3}AuP$^+$), and this triplet state has a strong absorption above 600 nm.[46] In contrast, no ^{1}AuP$^+$ intermediate could be distinguished in **OPE-AuP$^+$**, indicating that the intersystem crossing is faster than the time resolution of this experiment (∼100 fs) or that the spectral difference between ^{1}AuP$^+$ and ^{3}AuP$^+$ state of **OPE-AuP$^+$** is very small. Two time components are necessary for a good fit of the transient absorption data; a 2.5 ns component corresponding to the lifetime of the ^{3}AuP state and a 10 ps component, with small spectral changes. Comparing to other gold porphyrins,[46,47] it seems unlikely that the intersystem crossing of **OPE-AuP$^+$** is as slow as 10 ps, so it is more probable that this component corresponds to solvent and/or vibrational relaxation.[48]

Excitation of **ZnPc-OPE-AuP$^+$** at 555 nm results in the same initial absorption features above 600 nm as in the **OPE-AuP$^+$** reference (Figure 4c). However, within the duration of the laser pulse these features start to transform into the same spectra as

dx.doi.org/10.1021/ic3013552 | Inorg. Chem. XXXX, XXX, XXX−XXX

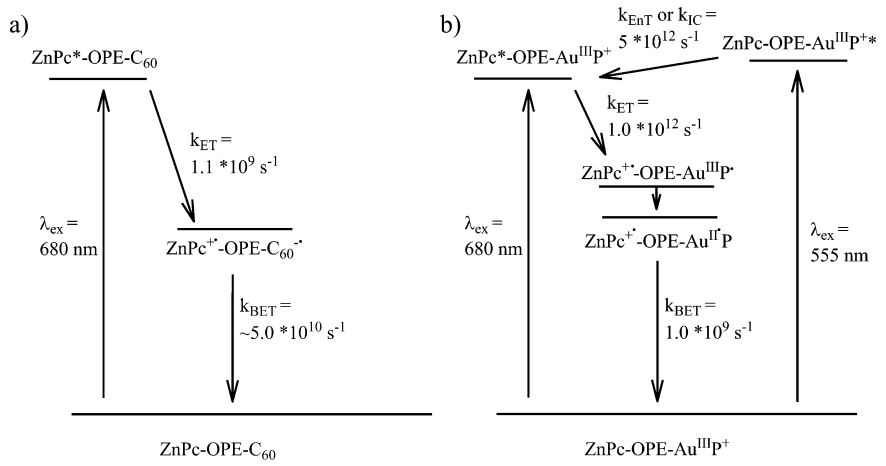

Figure 5. a) State diagram and rates of the reaction pathways in **ZnPc-OPE-C$_{60}$**. b) State diagram showing the reaction pathways in **ZnPc-OPE-AuP$^+$**.

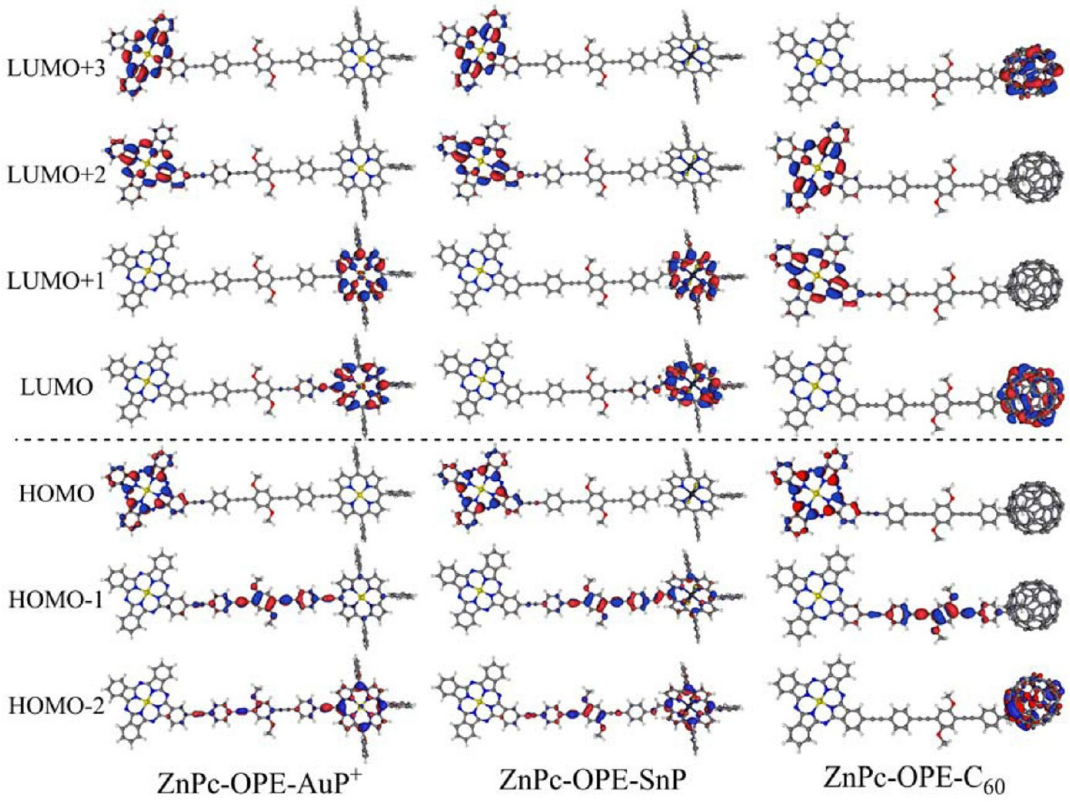

Figure 6. Representation of the calculated molecular orbitals for three donor–acceptor dyads. From bottom to top: HOMO-2, HOMO-1, HOMO, LUMO, LUMO+1, LUMO+2, and LUMO+3. See the SI for a representation of all relevant orbitals.

those observed immediately after excitation at 680 nm. The rapid (<1 ps) change is most easily seen as a fast decay of the AuP$^+$ excited state absorption at λ > 600 nm and a rapid formation of the ZnPc bleach around 680–710 nm (Figure 4d). A global fit analysis resulted in five time components: τ = 0.2 ps, 1.0 ps, 0.14 and 1.0 ns, and ∼∞ (held fixed). The 0.2 ps time component is assigned to a shift of excited state energy from a state that is mainly localized on the AuP$^+$-moiety to the same excited state as that produced upon 680 nm excitation. This is supported by the fact that the four longer time components and their corresponding decay associated difference spectra are the same as for ZnPc excitation at 680 nm (SI Figure S7). Summarily, excitation of ZnPc (at 680 nm) induces a very fast electron transfer (1 ps) followed by a slower charge recombination (1 ns) to the ground state, while excitation of AuP (at 555 nm) is accompanied by an extremely fast energy transfer to ZnPc (0.2 ps) and subsequently to charge separation and recombination to the ground state as upon ZnPc excitation (Figure 5b).

TD-DFT Calculations. To further investigate the strong interaction between the donor and acceptor moieties in **ZnPc-OPE-AuP$^+$** we turned to computational chemistry. Calculations of the absorption spectra, performed with time-dependent density functional theory (TD-DFT), managed to qualitatively

dx.doi.org/10.1021/ic3013552 | Inorg. Chem. XXXX, XXX, XXX–XXX

reproduce the absorption spectra of the investigated dyads. In the red part of the **ZnPc-OPE-AuP$^+$** spectrum, two intense vertical transitions were computed at 654 nm (f = 1.1) and 631 nm (f = 0.7). Both transitions are dominated by electronic excitation from HOMO (mainly ZnPc) to LUMO+2 and LUMO+3 (also ZnPc centered), see Figure 6. The two less intense transitions at 574 nm (f = 0.2) and 563 nm (f = 0.5) are related to the AuP$^+$ moiety. The latter transition is mainly from HOMO-2 to LUMO but also contains a small contribution related to a partial charge transfer from the bridge (HOMO-1) to the AuP$^+$ (LUMO). The situation is similar for **ZnPc-OPE-SnP**, but the SnP Q-band transition, computed at 593 nm (f = 0.4), has some contribution of charge transfer from the OPE bridge (HOMO-2) to the SnP (LUMO) (see SI for more detailed information on orbital contributions to the calculated transitions).

There are multiple bands in the Soret band region. In **ZnPc-OPE-SnP** the strongest ones, 432 nm (f = 4.0) and 398 nm (f = 1.4), are dominated by SnP localized $\pi-\pi^*$ transitions, but there is also a significant contribution of charge transfer from OPE to SnP. The same pattern can be seen in **ZnPc-OPE-AuP$^+$**, where the strongest transitions at 437 nm (f = 3.1) and 401 nm (f = 1.1) are mainly localized on the AuP$^+$ moiety. However, in this case there are not only contributions from OPE-to-acceptor charge transfer but also a smaller, but not insignificant, contribution from direct charge transfer from ZnPc to AuP$^+$ (HOMO to LUMO). These charge transfer interactions could be the reason for the strong broadening of the AuP$^+$ Soret band that is observed in the experimental spectra. Finally, as expected for **ZnPc-OPE-C$_{60}$**, the calculations indicate ZnPc based transitions in the visible range. Nevertheless, it is noticeable that the LUMO remains well centered on the C$_{60}$ accepting side. The break in conjugation between the fullerene and bridge introduced by the pyrrolidino functionality can also be seen in the molecular orbitals. In both **ZnPc-OPE-AuP$^+$** and **ZnPc-OPE-SnP**, there are high-lying occupied orbitals that cover both the OPE bridge and the accepting porphyrin (HOMO-2 for the former, HOMO-1 for the latter), whereas no such mixed orbitals can be found for **ZnPc-OPE-C$_{60}$**.

Comparison of Photoinduced Electron Transfer Rates. According to semiclassical Marcus theory (eq 2) electron transfer rates can be explained and predicted by four parameters: temperature (T), driving force (ΔG°), reorganization energy (λ), and electronic coupling (V_{DA}).[1b,49] We will discuss the observed trends in electron transfer rates between the three dyads within this framework.

$$k_{ET} = \sqrt{\frac{\pi}{\hbar^2 \lambda k_B T}}\, V_{DA}^2 \exp\left(\frac{-(\Delta G^\circ + \lambda)^2}{4\lambda k_B T}\right) \quad (2)$$

Driving forces for the three dyads were calculated from the values in Table 1 using the Weller equation[50] (Table 2, see SI for details). **ZnPc-OPE-C$_{60}$** has the largest driving force for photoinduced electron transfer (ΔG°_{PET}), followed by **ZnPc-OPE-SnP** and then **ZnPc-OPE-AuP$^+$**, while the trend for the rates for photoinduced electron transfer (k_{PET}) goes in the opposite direction, namely $k_{PET,\ \text{ZnPc-OPE-AuP+}} > k_{PET,\ \text{ZnPc-OPE-SnP}} > k_{PET,\ \text{ZnPc-OPE-C60}}$ (Table 2). The observation of opposite trends for rates and driving forces would be consistent if the reorganization energy were small (λ = ~0.6 eV), placing the electron transfer processes in the Marcus inverted region (i.e., $\lambda < -\Delta G^\circ$).[1b,2b,49] However, due to the long distance between donor and acceptor and the fairly polar solvent (PhCN: ε = 25)[51] we expect a larger reorganization energy (λ > 0.7 eV, see the SI for further discussion). This estimate of the reorganization energy suggests that the trend in electron transfer rates is not simply due to the Marcus inverted region effect.

Table 2. Summary of Rate Constants and Driving Forces for the Three Dyads

	k_{PET} (s^{-1})	ΔG°_{PET}[a] (eV)	k_{BET} (s^{-1})	ΔG°_{BET}[a] (eV)
ZnPc-OPE-C$_{60}$	1.1 × 10^9	−0.89	~5 × 10^{10}	−0.88
ZnPc-OPE-SnP[b]	7.6 × 10^{10}	−0.68	1.2 × 10^{10}	−1.09
ZnPc-OPE-AuP$^+$	1.0 × 10^{12}	−0.61	1.0 × 10^9	−1.16

[a]Driving forces for photoinduced electron transfer (ΔG°_{PET}) and the subsequent back electron transfer (ΔG°_{BET}) were estimated with the Weller equation, see the main text and the Supporting Information for more information. [b]Data from Fortage et al.[13a]

Instead the trend in photoinduced electron transfer rates could be explained by differences in electronic coupling. Trends in coupling strengths can be rationalized on the basis of both molecular structure and distribution of relevant orbitals. The break in conjugation between bridge and acceptor can explain why **ZnPc-OPE-C$_{60}$** appears to have the weakest electronic coupling. Similarly, that the PET rate is higher in **ZnPc-OPE-AuP$^+$** than in **ZnPc-OPE-SnP** can possibly be explained by the fact that the latter has a vinyl group instead of an ethynyl group as the linking unit between bridge and acceptor.[13b] Steric interaction between the vinyl group and the hydrogen at the β-position causes a ~40° dihedral angle between the double bond and the porphyrin plane, something which is expected to induce a weaker π-conjugation and hence a weaker electronic coupling (see the SI for calculated geometries).[13b,c,52] However, it should be noted that for both **ZnPc-OPE-SnP** and **ZnPc-OPE-AuP$^+$** the LUMO is partly spread out from the acceptor moiety onto the OPE bridge (Figure 6), indicating that both have a fairly strong electronic coupling between the acceptor and bridging moieties. Perturbation of the ground state absorption spectrum is another way to assess the magnitude of electronic coupling. We already know that interaction between donor and acceptor strongly perturb the absorption spectrum and the reduction potentials of **ZnPc-OPE-AuP$^+$** (*vide supra*). The effect of electronic coupling is less apparent in the absorption spectrum of **ZnPc-OPE-SnP**, but a small extra absorption can be seen in the region between 500 and 600 nm (SI Figure S1a). In contrast, the observed spectrum for **ZnPc-OPE-C$_{60}$** is an almost perfect match to the sum of the **ZnPc-OPE** and **C$_{60}$** references, which indicates fairly little electronic communication between ZnPc and C$_{60}$. This trend is further supported by the computational results above. The correlation between electron transfer rates and degree of perturbation of the absorption spectrum agrees with the hypothesis that it is the electronic coupling that is the main reason for the difference in reactivity between the three donor−acceptor dyads.

Comparison of Back Electron Transfer Rates. The rates for back electron transfer (k_{BET}) do not follow the same trend as the photoinduced electron transfer rates. **ZnPc-OPE-C$_{60}$**, which has the lowest forward rate, has the fastest back electron transfer rate. Faster back electron transfer rate compared to forward electron transfer is a fairly common feature in many donor−acceptor dyads,[13c,53] but it is difficult to explain why

dx.doi.org/10.1021/ic3013552 | Inorg. Chem. XXXX, XXX, XXX−XXX

this behavior only appears in the fullerene based dyad and not in the two porphyrin based systems. In an extensive review by G. Bottari et al.[15d] all the reported ZnPc-C_{60} dyads have charge separation rates that are faster than the charge recombination rates,[54] so **ZnPc-OPE-C_{60}** is a surprising exception also in that context.

A strong electronic coupling for forward electron transfer is often associated with a strong coupling for the back electron transfer, but **ZnPc-OPE-AuP$^+$** does not follow this pattern. Studies by Kadish and co-workers on the reduction of gold(III) porphyrins suggest a possible explanation.[18d,e] They found that depending on the substitution pattern of the gold porphyrin, the first reduction of an $Au^{III}P^+$ can occur on either the metal or on the porphyrin ring. In contrast, tin(IV) porphyrins, like most regular porphyrins, are expected to undergo ring based reductions.[55] Our hypothesis is that in both **ZnPc-OPE-AuP$^+$** and **ZnPc-OPE-SnP** photoinduced electron transfer results in an initial reduction of the porphyrin ring, However, for **ZnPc-OPE-AuP$^+$** the initial charge shifted state rapidly relaxes so that the gold ion is reduced instead of the porphyrin ring.[56] This would influence the back electron transfer in two ways.

The first effect of metal based reduction of AuP$^+$ is a change in reorganization energy. Kadish and co-workers reported that the reductive quenching of the triplet states of pyrene and phenanthrene by a gold porphyrin was associated with an unusual large reorganization energy (1.2 eV in PhCN), which can be compared to the typical value for metalloporphryins with ring centered reductions (~0.6 eV).[18e] However, for **ZnPc-OPE-AuP$^+$**, a similar increase in reorganization energy would actually be expected to result in a faster electron transfer rate (since $\lambda \approx -\Delta G°$), so this effect is not the major factor behind the slow back electron transfer.

The second effect is due to changes in the electronic coupling. If the excess electron is mainly situated in metal based orbitals it will interact less with the OPE bridge compared to if it were situated on the porphyrin ring. To confirm this hypothesis we utilized DFT to calculate the spin densities of the reduced state of the three different OPE-acceptor references. First, we optimized the geometries for the nonreduced bridge-acceptor fragments. Second, the nuclei were kept in the same position, but an extra electron was introduced. The spin density distribution that followed from this should approximate where the excess electron is situated directly after the electron is transferred ("unrelaxed" in Figure 7). Finally, the reduced bridge-acceptor fragment was relaxed to its lowest energy geometry. The resulting spin density should now show where the electron is situated in the relaxed charge-separated or charge-shifted state ("relaxed" in Figure 7). In the case of **ZnPc-OPE-AuP$^+$** one can clearly see the change from a ring-based reduction (unrelaxed) to a metal-centered reduction (relaxed). This strongly supports our hypothesis that the photoinduced electron transfer in **ZnPc-OPE-AuP$^+$** is first to a charge-shifted state that is situated on the rings of the donor and acceptor (**$Zn^{II}Pc^{+\bullet}$-OPE-$Au^{III}P^{\bullet}$**), which allows for a high coupling in the forward direction. The charge-shifted state then rapidly relaxes to a state where the excess electron in AuP is mainly on the gold ion (**$Zn^{II}Pc^{+\bullet}$-OPE-$Au^{II}P$**) where the electron has been "trapped". The same kind of stabilization is not possible in **ZnPc-OPE-SnP**, which may explain why the back electron transfer is about an order of magnitude faster than in **ZnPc-OPE-AuP$^+$**. This "trapping" mechanism might be part of the explanation to why dyad systems with AuP$^+$ tend to have long-lived charge shifted states.[13d,14c,18a,g]

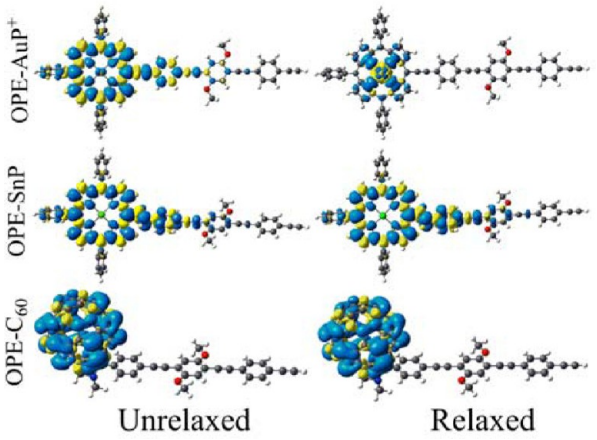

Figure 7. Spin density (contour threshold 0.0004 au) of the radical of the accepting side, using an unrelaxed or relaxed geometry (see text for more details). From top to bottom: **OPE-AuP$^+$**, **OPE-SnP**, and the **OPE-C_{60}**. Note how the spin density of relaxed AuP is centered on the metal, while for relaxed SnP it is spread out over the π-conjugated system.

CONCLUSIONS

We have shown that both **ZnPc-OPE-AuP$^+$** and **ZnPc-OPE-C_{60}** in PhCN undergo photoinduced electron transfer. For **ZnPc-OPE-C_{60}** the back electron transfer is much faster ($k_{BET} \approx 5 \times 10^{10}$ s^{-1}) than the photoinduced forward reaction ($k_{PET} = 1.1 \times 10^9$ s^{-1}), which prevents build up of the desired charge-separated state. In contrast, **ZnPc-OPE-AuP$^+$** undergoes ultrafast, long-range photoinduced electron transfer over an edge-to-edge distance of 23 Å with $k_{PET} = 1.0 \times 10^{12}$ s^{-1}, followed by recombination with $k_{BET} = 1.0 \times 10^9$ s^{-1}. The high forward rate is due to strong electronic coupling, which is also reflected in a strong perturbation of the steady-state absorption spectrum. The comparably long-lived charge-shifted state is formed because the reduced gold porphyrin relaxes from a $Au^{III}P^{\bullet}$ radical to a $Au^{II}P$ species, with the excess electron density localized on the metal. The metal-centered reduced species interacts less with the bridge and the electronic interaction with the hole on ZnPc becomes smaller. **ZnPc-OPE-SnP**, which is structurally very similar, does not undergo the same kind of metal based reduction. In this case, the rate for back electron transfer is an order of magnitude larger. This information may be useful for the design of multichromophoric systems that undergoes very fast photoinduced electron transfer and still have a significant lifetime for the charge-separated state.

ASSOCIATED CONTENT

Supporting Information

Additional spectroscopic data, details on calculations of rate constants, driving forces and reorganization energies, Cartesian coordinates for the three dyad systems, simulated UV/vis spectra, list of the main vertical transitions and corresponding orbital composition, and representation of all relevant molecular orbitals. This material is available free of charge via the Internet at http://pubs.acs.org.

AUTHOR INFORMATION

Corresponding Author

*Phone: +33 (0)2 51 12 54 29. Fax: +33 (0)2 51 12 54 02. E-mail: Denis.Jacquemin@univ-nantes.fr (D.J.) and Fabrice.

dx.doi.org/10.1021/ic3013552 | Inorg. Chem. XXXX, XXX, XXX−XXX

Odobel@univ-nantes.fr (F.O.). Phone: +46-18-471 3648; Fax: +46-18-471 6844; E-mail: Leif.Hammarstrom@fotomol.uu.se (L.H.).

Notes

The authors declare no competing financial interest.

■ ACKNOWLEDGMENTS

We thank Dr. Susanne Karlsson for providing valuable input to this project while working at Uppsala University. Financial support from the following agencies is gratefully acknowledged: Knut and Alice Wallenberg foundation, the Swedish Reaseach Council, the Agence Nationale de la Recherche (ANR) "PhotoCumElec" program, ACI jeune chercheur, and the European Community for the COST D35 program. D. Jacquemin acknowledges the *Région des Pays de la Loire* and the European Research Council (ERC) for financial support in the framework of a *recrutement sur poste stratégique* and a Starting Grant (Marches -278845), respectively. The theoretical part of this research used resources from the following: 1) the Interuniversity Scientific Computing Facility located at the University of Namur, Belgium, which is supported by the F.R.S.-FNRS under convention No. 2.4617.07, 2) the GENCI-CINES/IDRIS (Grant c2011085117), and 3) the CCIPL (*Centre de Calcul Intensif des Pays de Loire*).

■ REFERENCES

(1) (a) Gray, H. B.; Winkler, J. R. *Proc. Natl. Acad. Sci. U.S.A.* **2005**, *102*, 3534−3539. (b) Marcus, R. A.; Sutin, N. *Biochim. Biophys. Acta, Rev. Bioenerg.* **1985**, *811*, 265−322.

(2) (a) Wasielewski, M. R. *Chem. Rev.* **1992**, *92*, 435−461. (b) Closs, G. L.; Miller, J. R. *Science* **1988**, *240*, 440−447.

(3) (a) Tommos, C.; Babcock, G. T. *Acc. Chem. Res.* **1998**, *31*, 18−25. (b) Ort, D. R.; Yocum, C. F.; Heichel, I. F. *Oxygenic Photosynthesis: The Light Reactions*; Kluwer Academic Publisher: Dordrecht, The Netherlands, 1996; *Vol. 4*.

(4) (a) Lubitz, W.; Reijerse, E.; van Gastel, M. *Chem. Rev.* **2007**, *107*, 4331−4365. (b) Pandelia, M.-E.; Nitschke, W.; Infossi, P.; Giudici-Orticoni, M.-T.; Bill, E.; Lubitz, W. *Proc. Natl. Acad. Sci. U.S.A.* **2011**.

(5) Gray, H. B.; Winkler, J. R. *Biochim. Biophys. Acta, Bioenerg.* **2010**, *1797*, 1563−1572.

(6) (a) Brédas, J.-L.; Norton, J. E.; Cornil, J.; Coropceanu, V. *Acc. Chem. Res.* **2009**, *42*, 1691−1699. (b) Inganäs, O.; Zhang, F.; Andersson, M. R. *Acc. Chem. Res.* **2009**, *42*, 1731−1739. (c) Roncali, J. *Acc. Chem. Res.* **2009**, *42*, 1719−1730.

(7) (a) Grätzel, M. *Acc. Chem. Res.* **2009**, *42*, 1788−1798. (b) O'Regan, B. C.; Durrant, J. R. *Acc. Chem. Res.* **2009**, *42*, 1799−1808. (c) O'Regan, B.; Grätzel, M. *Nature* **1991**, *353*, 737−740. (d) Hagfeldt, A.; Grätzel, M. *Acc. Chem. Res.* **2000**, *33*, 269−277.

(8) (a) Youngblood, W. J.; Lee, S.-H. A.; Maeda, K.; Mallouk, T. E. *Acc. Chem. Res.* **2009**, *42*, 1966−1973. (b) Gust, D.; Moore, T. A.; Moore, A. L. *Acc. Chem. Res.* **2009**, *42*, 1890−1898. (c) Magnuson, A.; Anderlund, M.; Johansson, O.; Lindblad, P.; Lomoth, R.; Polivka, T.; Ott, S.; Stensjö, K.; Styring, S.; Sundström, V.; Hammarström, L. *Acc. Chem. Res.* **2009**, *42*, 1899−1909.

(9) Tour, J. M. *Acc. Chem. Res.* **2000**, *33*, 791−804.

(10) (a) Wagner, R. W.; Lindsey, J. S. *J. Am. Chem. Soc.* **1994**, *116*, 9759−9760. (b) Wagner, R. W.; Lindsey, J. S.; Seth, J.; Palaniappan, V.; Bocian, D. F. *J. Am. Chem. Soc.* **1996**, *118*, 3996−3997.

(11) (a) Gust, D.; Moore, T. A.; Moore, A. L. *Chem. Commun.* **2006**, 1169−1178. (b) Balzani, V. *Photochem. Photobiol. Sci.* **2003**, *2*, 459−476. (c) Aviram, A.; Ratner, M. A. *Chem. Phys. Lett.* **1974**, *29*, 277−283. (d) Debreczeny, M. P.; Svec, W. A.; Wasielewski, M. R. *Science* **1996**, *274*, 584−587. (e) Green, J. E.; Wook Choi, J.; Boukai, A.; Bunimovich, Y.; Johnston-Halperin, E.; DeIonno, E.; Luo, Y.; Sheriff, B. A.; Xu, K.; Shik Shin, Y.; Tseng, H.-R.; Stoddart, J. F.; Heath, J. R. *Nature* **2007**, *445*, 414−417. (f) Chen, J.; Reed, M. A.; Rawlett, A. M.; Tour, J. M. *Science* **1999**, *286*, 1550−1552.

(12) (a) Winters, M. U.; Pettersson, K.; Mårtensson, J.; Albinsson, B. *Chem.–A Eur. J.* **2005**, *11*, 562−573. (b) de la Torre, G.; Giacalone, F.; Segura, J. L.; Martín, N.; Guldi, D. M. *Chem.–Eur. J.* **2005**, *11*, 1267−1280. (c) Giacalone, F.; Segura, J. L.; Martín, N.; Guldi, D. M. *J. Am. Chem. Soc.* **2004**, *126*, 5340−5341. (d) Giacalone, F.; Segura, J. L.; Martín, N.; Ramey, J.; Guldi, D. M. *Chem.–Eur. J.* **2005**, *11*, 4819−4834. (e) Davis, W. B.; Ratner, M. A.; Wasielewski, M. R. *J. Am. Chem. Soc.* **2001**, *123*, 7877−7886. (f) Davis, W. B.; Svec, W. A.; Ratner, M. A.; Wasielewski, M. R. *Nature* **1998**, *396*, 60−63. (g) Odobel, F.; Fortage, J. *C. R. Chim.* **2009**, *12*, 437−449.

(13) (a) Fortage, J.; Göransson, E.; Blart, E.; Becker, H.-C.; Hammarström, L.; Odobel, F. *Chem. Commun.* **2007**, 4629−4631. (b) Odobel, F.; Suresh, S.; Blart, E.; Nicolas, Y.; Quintard, J.-P.; Janvier, P.; Le Questel, J.-Y.; Illien, B.; Rondeau, D.; Richomme, P.; Häupl, T.; Wallin, S.; Hammarström, L. *Chem.–A Eur. J.* **2002**, *8*, 3027−3046. (c) Redmore, N. P.; Rubtsov, I. V.; Therien, M. J. *J. Am. Chem. Soc.* **2003**, *125*, 8769−8778. (d) Fortage, J.; Boixel, J.; Blart, E.; Hammarström, L.; Becker, H. C.; Odobel, F. *Chem.–Eur. J.* **2008**, *14*, 3467−3480. (e) Lembo, A.; Tagliatesta, P.; Guldi, D. M.; Wielopolski, M.; Nuccetelli, M. *J. Phys. Chem. A* **2009**, *113*, 1779−1793.

(14) (a) Fukuzumi, S. Electron Transfer Chemistry of Porphyrins and Metalloporphyrins. In *Porphyrin Handbook*; Kadish, K. M., Smith, K. M., Guilard, R., Eds.; Academic Press: New York, USA, 1999; pp 115−152; (b) Mataga, N.; Chosrowjan, H.; Taniguchi, S. *J. Photochem. Photobiol., C* **2005**, *6*, 37−79. (c) Wiberg, J.; Guo, L.; Pettersson, K.; Nilsson, D.; Ljungdahl, T.; Mårtensson, J.; Albinsson, B. *J. Am. Chem. Soc.* **2006**, *129*, 155−163. (d) Holten, D.; Bocian, D. F.; Lindsey, J. S. *Acc. Chem. Res.* **2001**, *35*, 57−69. (e) Kuciauskas, D.; Lin, S.; Seely, G. R.; Moore, A. L.; Moore, T. A.; Gust, D.; Drovetskaya, T.; Reed, C. A.; Boyd, P. D. W. *J. Phys. Chem.* **1996**, *100*, 15926−15932. (f) Pettersson, K.; Wiberg, J.; Ljungdahl, T.; Mårtensson, J.; Albinsson, B. *J. Phys. Chem. A* **2005**, *110*, 319−326. (g) Guldi, D. M. *Chem. Soc. Rev.* **2002**, *31*, 22−36. (h) Imahori, H. *Org. Biomol. Chem.* **2004**, *2*, 1425−1433. (i) Osuka, A.; Tanabe, N.; Kawabata, S.; Yamazaki, I.; Nishimura, Y. *J. Org. Chem.* **1995**, *60*, 7177−7185. (j) Nakano, A.; Osuka, A.; Yamazaki, T.; Nishimura, Y.; Akimoto, S.; Yamazaki, I.; Itaya, A.; Murakami, M.; Miyasaka, H. *Chem.–A Eur. J.* **2001**, *7*, 3134−3151. (k) Gust, D.; Moore, T. A.; Moore, A. L. *Acc. Chem. Res.* **1993**, *26*, 198−205. (l) Kim, D.; Osuka, A. *Acc. Chem. Res.* **2004**, *37*, 735−745.

(15) (a) Lo, P.-C.; Leng, X.; Ng, D. K. P. *Coord. Chem. Rev.* **2007**, *251*, 2334−2353. (b) Maligaspe, E.; Kumpulainen, T.; Lemmetyinen, H.; Tkachenko, N. V.; Subbaiyan, N. K.; Zandler, M. E.; D'Souza, F. *J. Phys. Chem. A* **2009**, *114*, 268−277. (c) Martinez-Diaz, M. V.; de la Torre, G.; Torres, T. *Chem. Commun.* **2010**, *46*, 7090−7108. (d) Bottari, G.; de la Torre, G.; Guldi, D. M.; Torres, T. *Chem. Rev.* **2010**, *110*, 6768−6816.

(16) (a) Gonzalez-Cabello, A.; Vazquez, P.; Torres, T. *J. Organomet. Chem.* **2001**, *637*−*639*, 751−756. (b) Sutton, J. M.; Boyle, R. W. *Chem. Commun.* **2001**, 2014−2015. (c) Garcia-Frutos, E. M.; O'Flaherty, S. M.; Maya, E. M.; De La Torre, G.; Blau, W.; Vazquez, P.; Torres, T. *J. Mater. Chem.* **2003**, *13*, 749−753. (d) Imahori, H.; Umeyama, T.; Ito, S. *Acc. Chem. Res.* **2009**, *42*, 1809−1818.

(17) (a) Hardin, B. E.; Hoke, E. T.; Armstrong, P. B.; Yum, J.-H.; Comte, P.; Torres, T.; Frechet, J. M. J.; Nazeeruddin, M. K.; Gratzel, M.; McGehee, M. D. *Nat. Photonics* **2009**, *3*, 406−411. (b) Brown, M. D.; Parkinson, P.; Torres, T.; Miura, H.; Herz, L. M.; Snaith, H. J. *J. Phys. Chem. C* **2011**, *115*, 23204−23208. (c) Gonzalez-Cabello, A.; Vazquez, P.; Torres, T.; Guldi, D. M. *J. Org. Chem.* **2003**, *68*, 8635−8642.

(18) (a) Harriman, A.; Heitz, V.; Sauvage, J. P. *J. Phys. Chem.* **1993**, *97*, 5940−5946. (b) Brun, A. M.; Harriman, A.; Heitz, V.; Sauvage, J. P. *J. Am. Chem. Soc.* **1991**, *113*, 8657−8663. (c) Kilså, K.; Kajanus, J.; Macpherson, A. N.; Mårtensson, J.; Albinsson, B. *J. Am. Chem. Soc.* **2001**, *123*, 3069−3080. (d) Kadish, K. M.; E, W.; Ou, Z.; Shao, J.; Sintic, P. J.; Ohkubo, K.; Fukuzumi, S.; Crossley, M. J. *Chem. Commun.* **2002**, 356−357. (e) Ou, Z.; Kadish, K. M.; E, W.; Shao, J.; Sintic, P. J.;

Ohkubo, K.; Fukuzumi, S.; Crossley, M. J. *Inorg. Chem.* **2004**, *43*, 2078−2086. (f) Fortage, J.; Boixel, J.; Blart, E.; Becker, H. C.; Odobel, F. *Inorg. Chem.* **2009**, *48*, 518−526. (g) Andersson, M.; Linke, M.; Chambron, J.-C.; Davidsson, J.; Heitz, V.; Hammarström, L.; Sauvage, J.-P. *J. Am. Chem. Soc.* **2002**, *124*, 4347−4362.

(19) Prato, M.; Maggini, M. *Acc. Chem. Res.* **1998**, *31*, 519−526.

(20) (a) Donhauser, Z. J.; Mantooth, B. A.; Kelly, K. F.; Bumm, L. A.; Monnell, J. D.; Stapleton, J. J.; Price, D. W.; Rawlett, A. M.; Allara, D. L.; Tour, J. M.; Weiss, P. S. *Science* **2001**, *292*, 2303−2307. (b) Weber, H. B.; Reichert, J.; Weigend, F.; Ochs, R.; Beckmann, D.; Mayor, M.; Ahlrichs, R.; Löhneysen, H. v. *Chem. Phys.* **2002**, *281*, 113−125.

(21) Ik Yang, S.; Lammi, R. K.; Prathapan, S.; Miller, M. A.; Seth, J.; Diers, J. R.; Bocian, D. F.; Lindsey, J. S.; Holten, D. *J. Mater. Chem.* **2001**, *11*, 2420−2430.

(22) Gonzalez-Rojano, N.; Arias-Marin, E.; Navarro-Rodriguez, D.; Weidner, S. *Synlett* **2005**, 1259−1262.

(23) Chaignon, F.; Torroba, J.; Blart, E.; Borgström, M.; Hammarström, L.; Odobel, F. *New J. Chem.* **2005**, *29*, 1272−1284.

(24) Maya, E. M.; Vazquez, P.; Torres, T. *Chem.–Eur. J.* **1999**, *5*, 2004−2013.

(25) Connelly, N. G.; Geiger, W. E. *Chem. Rev.* **1996**, *96*, 877−910.

(26) Rhile, I. J.; Markle, T. F.; Nagao, H.; DiPasquale, A. G.; Lam, O. P.; Lockwood, M. A.; Rotter, K.; Mayer, J. M. *J. Am. Chem. Soc.* **2006**, *128*, 6075−6088.

(27) Habenicht, A.; Hjelm, J.; Mukhtar, E.; Bergström, F.; Johansson, L. B. Å. *Chem. Phys. Lett.* **2002**, *354*, 367−375.

(28) Petersson, J.; Eklund, M.; Davidsson, J.; Hammarström, L. *J. Phys. Chem. B* **2010**, *114*, 14329−14338.

(29) WaveMetrics, Igor Pro 5.

(30) Frisch, M. J.; Trucks, G. W.; Schlegel, H. B.; Scuseria, G. E.; Robb, M. A.; Cheeseman, J. R.; Scalmani, G.; Barone, V.; Mennucci, B.; Petersson, G. A.; Nakatsuji, H.; Caricato, M.; Li, X.; Hratchian, H. P.; Izmaylov, A. F.; Bloino, J.; Zheng, G.; Sonnenberg, J. L.; Hada, M.; Ehara, M.; Toyota, K.; Fukuda, R.; Hasegawa, J.; Ishida, M.; Nakajima, T.; Honda, Y.; Kitao, O.; Nakai, H.; Vreven, T.; Montgomery, J. A.; Peralta, J. E.; Ogliaro, F.; Bearpark, M.; Heyd, J. J.; Brothers, E.; Kudin, K. N.; Staroverov, V. N.; Kobayashi, R.; Normand, J.; Raghavachari, K.; Rendell, A.; Burant, J. C.; Lyengar, S. S.; Tomasi, J.; Cossi, M.; Rega, N.; Millam, J. M. a. K, M.; a. K, J. E.; a. C, J. B.; a. B, V.; a. A, C.; a. J, J.; a. R. *Gaussian 09 Revision A.02*; Gaussian Inc.: Wallingford, CT, 2009.

(31) Jacquemin, D.; Perpète, E. A.; Ciofini, I.; Adamo, C. *Acc. Chem. Res.* **2009**, *42*, 326−334.

(32) Adamo, C.; Barone, V. J. *Chem. Phys.* **1999**, *110*, 6158−6170.

(33) Tomasi, J.; Mennucci, B.; Cammi, R. *Chem. Rev.* **2005**, *105*, 2999−3094.

(34) Yanai, T.; Tew, D. P.; Handy, N. C. *Chem. Phys. Lett.* **2004**, *393*, 51−56.

(35) (a) Peach, M. J. G.; Benfield, P.; Helgaker, T.; Tozer, D. J. J. *Chem. Phys.* **2008**, *128*, 044118. (b) Goerigk, L.; Grimme, S. J. *Chem. Phys.* **2010**, *132*, 184103. (c) Jacquemin, D.; Perpète, E. A.; Ciofini, I.; Adamo, C. *J. Chem. Theory Comput.* **2009**, *5*, 2420−2435.

(36) Cossi, M.; Barone, V. J. *Chem. Phys.* **2001**, *115*, 4708−4717.

(37) Tagmatarchis, N.; Prato, M. *Synlett* **2003**, 768−779.

(38) (a) González-Rodríguez, D.; Claessens, C. G.; Torres, T.; Liu, S.; Echegoyen, L.; Vila, N.; Nonell, S. *Chem.–A Eur. J.* **2005**, *11*, 3881−3893. (b) Jiménez, Á. J.; Spänig, F.; Rodríguez-Morgade, M. S.; Ohkubo, K.; Fukuzumi, S.; Guldi, D. M.; Torres, T. *Org. Lett.* **2007**, *9*, 2481−2484.

(39) (a) Lin, V.; DiMagno, S.; Therien, M. *Science* **1994**, *264*, 1105−1111. (b) Lin, V. S. Y.; Therien, M. J. *Chem.–A Eur. J.* **1995**, *1*, 645−651. (c) Shediac, R.; Gray, M. H. B.; Uyeda, H. T.; Johnson, R. C.; Hupp, J. T.; Angiolillo, P. J.; Therien, M. J. *J. Am. Chem. Soc.* **2000**, *122*, 7017−7033. (d) Winters, M. U.; Kärnbratt, J.; Eng, M.; Wilson, C. J.; Anderson, H. L.; Albinsson, B. *J. Phys. Chem. C* **2007**, *111*, 7192−7199.

(40) Two longer lifetimes, 1.8 ns and ∞ (both held fixed), were needed for a satisfactory global fit of the visible data. The 1.8 ns component corresponds to the decay of the singlet excited state of the small unquenched fraction of ZnPc observed in the time-resolved emission measurements (1.8 ns). The "infinite" component comes from the very long-lived ^{3}ZnPc, which forms in a significant amount from the ^{1}ZnPc state due to the slow electron transfer rate, which allows the intersystem crossing to compete.

(41) Since we used a cutoff filter to block visible light, we can exclude that the absorption in the NIR is an artifact due to second order diffraction of visible light.

(42) Detection of the ZnPc+ radical signal at ∼850 nm was precluded due to instrument limitations to detect in around 800 nm (see the Experimental Section).

(43) Guldi, D. M.; Prato, M. *Acc. Chem. Res.* **2000**, *33*, 695−703.

(44) The spectral changes in the DADS are blue-shifted about 20 nm compared to the features in the simulated charge separated state (Figure 2b and SI Figure S7c). Most likely this mismatch is due to the strong interaction between ZnPc and AuP+, which perturbs the bands in the Soret band region. Since the Soret band region in the ground state could not be fully described by a sum of ZnPc and AuP+ it is reasonable to expect that a ZnPc$^{\bullet+}$-OPE-Au^{III}P and ZnPc-OPE-Au^{II}P could not fully describe the charge separated state, ZnPc$^{\bullet+}$-OPE-Au^{II}P.

(45) The small fraction of unquenched 1ZnPc and the spectral similarity beteween the 1ZnPc and 3ZnPc makes it difficult to resolve the 1.8 ns time component with fs-TA. This is in contrast to the TCSPC measurement where there are no interfering signals from the ZnPc units that undergo photoinduces electron transfer (i.e., the majority of ZnPc).

(46) Andréasson, J.; Kodis, G.; Lin, S.; Moore, A. L.; Moore, T. A.; Gust, D.; Mårtensson, J.; Albinsson, B. *Photochem. Photobiol.* **2002**, *76*, 47−50.

(47) Eng, M. P.; Ljungdahl, T.; Andréasson, J.; Mårtensson, J.; Albinsson, B. *J. Phys. Chem. A* **2005**, *109*, 1776−1784.

(48) (a) Mizutani, Y.; Kitagawa, T. *J. Mol. Liq.* **2001**, *90*, 233−242. (b) Pigliucci, A.; Duvanel, G.; Daku, L. M. L.; Vauthey, E. *J. Phys. Chem. A* **2007**, *111*, 6135−6145. (c) Petersson, J.; Eklund, M.; Davidsson, J.; Hammarström, L. *J. Phys. Chem. B* **2010**, *114*, 14329−14338.

(49) Marcus, R. A. *J. Chem. Phys.* **1965**, *43*, 679−701.

(50) (a) Rehm, D.; Weller, A. *Isr. J. Chem.* **1970**, *8*, 259−271. (b) Weller, A. *Z. Phys. Chem.* **1982**, *133*, 93−98.

(51) Montalti, M.; Credi, A.; Prodi, L.; Gandolfi, M. T. *Handbook of Photochemistry*, 3rd ed.; CRC Press, Taylor & Francis: Boca Raton, FL, USA, 2006.

(52) (a) Wallin, S.; Hammarström, L.; Blart, E.; Odobel, F. *Photochem. Photobiol. Sci.* **2006**, *5*, 828−834. (b) Eng, M. P.; Albinsson, B. *Chem. Phys.* **2009**, *357*, 132−139.

(53) (a) Fortage, J.; Göransson, E.; Blart, E.; Becker, H.-C.; Hammarström, L.; Odobel, F. *Chem. Commun.* **2007**, 4629−4631. (b) Kirmaier, C.; Yang, S. I.; Prathapan, S.; Miller, M. A.; Diers, J. R.; Bocian, D. F.; Lindsey, J. S.; Holten, D. *Res. Chem. Intermed.* **2002**, *28*, 719−740. (c) Palacios, R. E.; Kodis, G.; Herrero, C.; Ochoa, E. M.; Gervaldo, M.; Gould, S. L.; Kennis, J. T. M.; Gust, D.; Moore, T. A.; Moore, A. L. *J. Phys. Chem. B* **2006**, *110*, 25411−25420.

(54) (a) Gouloumis, A.; de la Escosura, A.; Vázquez, P.; Torres, T.; Kahnt, A.; Guldi, D. M.; Neugebauer, H.; Winder, C.; Drees, M.; Sariciftci, N. S. *Org. Lett.* **2006**, *8*, 5187−5190. (b) Guldi, D. M.; Gouloumis, A.; Vázquez, P.; Torres, T.; Georgakilas, V.; Prato, M. *J. Am. Chem. Soc.* **2005**, *127*, 5811−5813. (c) Guldi, D. M.; Gouloumis, A.; Vazquez, P.; Torres, T. *Chem. Commun.* **2002**, 2056−2057. (d) Isosomppi, M.; Tkachenko, N. V.; Efimov, A.; Vahasalo, H.; Jukola, J.; Vainiotalo, P.; Lemmetyinen, H. *Chem. Phys. Lett.* **2006**, *430*, 36−40. (e) Kahnt, A.; Guldi, D. M.; de la Escosura, A.; Martinez-Diaz, M. V.; Torres, T. *J. Mater. Chem.* **2008**, *18*, 77−82. (f) Quintiliani, M.; Kahnt, A.; Vazquez, P.; Guldi, D. M.; Torres, T. *J. Mater. Chem.* **2008**, *18*, 1542−1546.

(55) Kalyanasundaram, K. *Photochemistry of Polypyridine and Porphyrin Complexes*; Academic Press: London, UK, 1992.

(56) DFT indicated no significant barrier, so we assume that this relaxation process occurs on a subps time scale. The unknown liftime (∼120 ps), which was found in the global analysis, is to slow to be a plausible candidate for this reaction.